Chapter 12

Optical Manipulation of Ultracold Atoms

G. Juzeliūnas[1] *and P. Öhberg*[2]

[1]*Institute of Theoretical Physics and Astronomy of Vilnius University, Lithuania*
[2]*Heriot-Watt University, United Kingdom*

12.1 BACKGROUND

The concept of using light to manipulate ensembles of, or indeed individual, atoms, goes back a long time. From Maxwell's theory of electromagnetism, it became clear that light carries a momentum that can be transferred to particles [1]. Classically, a light beam will induce forces on a dipole. These forces depend upon the shape of the light beam—both the intensity and the phase. With the advent of the laser in the 1960s, it became possible to address in an unprecedented way the mechanical forces on atoms where the internal level structure of the atoms was exploited. This opened a path toward laser cooling and trapping atoms, where, in particular, the quantum mechanical nature of the atoms needed to be taken into account [2–4].

Optical manipulation of quantum objects has come a long way since the early attempts a century ago to manipulate the dynamics of thermal gases. In this chapter, we will first briefly review the mechanisms for trapping ensembles of ultracold atoms. These techniques will then be applied to neutral atoms that form a Bose–Einstein condensate. The optical trap will form the basis for manipulating the cold atoms where we rely on the coherent nature of the ultracold sample of atoms and the intensity of the light.

Subsequently, we will discuss a situation where the phase and the intensity of the incident light both play a crucial role. Here, we will consider a different kind of op-

STRUCTURED LIGHT AND ITS APPLICATIONS

tical manipulation where the laser fields are applied to induce vector and scalar potentials acting on atoms. The induced potentials have a geometric nature and depend exclusively upon the relative intensity and relative phase of the laser beams involved rather than on their absolute intensity. The approach relies on the ability to prepare the atoms in superpositions of the internal energy states of the atom. Interestingly, this technique provides a way to optically induce an effective magnetic field acting on electrically neutral atoms. This happens if the applied laser fields have a nontrivial topology, e.g., if they carry an orbital angular momentum along the propagation direction [5–7].

12.2 OPTICAL FORCES AND ATOM TRAPS

It was known since the time of Maxwell that light exerts a force on classical dipoles. The resulting force does indeed depend on the gradient of the amplitude and phase of the light [8],

$$m\ddot{\mathbf{R}} = \mathbf{d}\cdot(\nabla\mathbf{E}) = \mathbf{d}\cdot(\nabla\xi + \xi\nabla\theta)e^{i(\omega t+\theta)}, \tag{1}$$

where m is the mass of the dipole, $\mathbf{d}$ is the dipole moment, and $\mathbf{E}(\mathbf{R},t) = \epsilon\xi(\mathbf{R})e^{i(\omega t+\theta(\mathbf{R}))}$ is the electric field with the corresponding amplitude ξ, polarization ϵ, phase θ, and frequency ω.

An atom can be considered as a prototype dipole. For this purpose, let us restrict ourselves to two energy levels, as shown in Figure 12.1. Our goal is to describe the atom quantum mechanically, but allow the light field to be classical. The Hamiltonian for the atom is then

$$H = \frac{\mathbf{P}^2}{2m} + \hat{H}_0 - \mathbf{d}\cdot\mathbf{E}(\mathbf{R},t), \tag{2}$$

where $\mathbf{P}^2/2m$ is the kinetic energy associated with the center of mass motion of the atom, $\hat{H}_0$ is the Hamiltonian for the unperturbed internal motion, and $\mathbf{d}\cdot\mathbf{E}(\mathbf{R},t)$ is the interaction between the atom and the light field, which is based upon the dipole approximation. With the Hamiltonian from equation (2) and the Ehrenfest theorem, we obtain the expression for the force

$$F = m\ddot{\mathbf{r}} = \left\langle\nabla(\mathbf{d}\cdot\mathbf{E})\right\rangle = \langle\mathbf{d}\cdot\epsilon\rangle\nabla\xi(\mathbf{r},t), \tag{3}$$

where $\mathbf{r} = \langle\mathbf{R}\rangle$ and $\xi(\mathbf{r},t) = \xi(\mathbf{r})e^{i(\omega t+\theta(\mathbf{r}))}$. On the right side above, we have assumed that the force is uniform across the atomic wave packet. For a thorough discussion, we refer to references [9,10,2,8].

The two-level atom driven by a laser has been studied extensively [9–12,8]. In order to obtain an expression for the force acting on the atom, we need to calculate

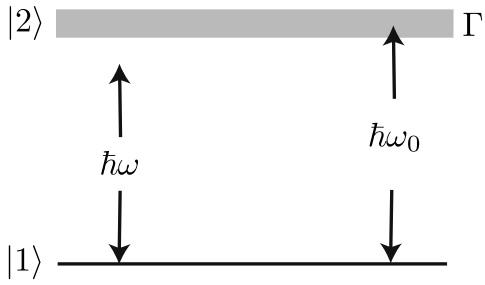

Figure 12.1 The atom is described as a two level system with energy difference $\hbar\omega_0$ between stat $|1\rangle$ and $|2\rangle$, and the frequency of the driving laser by ω. The decay rate of the excited state $|2\rangle$ is given by Γ.

the response of the atom to the light, i.e., the susceptibility or polarization, $\langle \mathbf{d} \cdot \boldsymbol{\epsilon} \rangle$. For this, we assume a monochromatic field of the form

$$\xi(\mathbf{r}, t) = \frac{1}{2} E(\mathbf{r}) e^{i(\theta(\mathbf{r}) + \omega t)}, \tag{4}$$

where $E(\mathbf{r})$ is the amplitude, ω is the laser frequency, and θ is a space-dependent phase factor. From the Schrödinger equation, we obtain the two coupled equations for the probability amplitudes C_1 and C_2 for the atom to be in state $|1\rangle$ and $|2\rangle$, respectively. By choosing a rotating frame according to

$$C_1 = D_1 e^{i\frac{1}{2}(\delta t + \theta)}, \tag{5}$$

$$C_2 = D_2 e^{-i\frac{1}{2}(\delta t + \theta)}, \tag{6}$$

we obtain the equations [9]

$$i\dot{D}_1 = \frac{1}{2}(\delta + \dot{\theta}) D_1 - \frac{\Omega}{2} D_2, \tag{7}$$

$$i\dot{D}_2 = -\frac{1}{2}(\delta + \dot{\theta}) D_2 - \frac{\Omega}{2} D_1. \tag{8}$$

In deriving the equations for D_1 and D_2, we have introduced the detuning $\delta = \omega - \omega_0$ and used the rotating wave approximation where rapidly oscillating terms are neglected [12]. The dipole moment d for the transition between state 1 and 2 is given by $d = \langle 1 | \mathbf{d} \cdot \boldsymbol{\epsilon} | 2 \rangle$, and the Rabi frequency is defined by

$$\Omega = \frac{d E(t)}{\hbar}. \tag{9}$$

It is convenient to introduce the density matrix at this stage, which is defined as $\rho_{nm} = C_n C_m^*$ or $\sigma_{nm} = D_n D_m^*$ with

$$\rho_{11} = \sigma_{11}, \tag{10}$$

$$\rho_{22} = \sigma_{22}, \tag{11}$$

$$\rho_{12} = \sigma_{12} e^{i(\theta+\omega t)}, \tag{12}$$

$$\rho_{21} = \sigma_{21} e^{-i(\theta+\omega t)}. \tag{13}$$

From equations (7) and (8), we can see that the matrix elements of the density matrix obey

$$\dot{\sigma}_{11} = -\frac{i}{2}\Omega(\sigma_{12} - \sigma_{21}) + \Gamma\sigma_{22}, \tag{14}$$

$$\dot{\sigma}_{22} = \frac{i}{2}\Omega(\sigma_{12} - \sigma_{21}) - \Gamma\sigma_{22}, \tag{15}$$

$$\dot{\sigma}_{12} = -i(\delta + \dot{\theta})\sigma_{12} + \frac{i}{2}\Omega(\sigma_{22} - \sigma_{11}) - \frac{1}{2}\Gamma\sigma_{12}, \tag{16}$$

where we have introduced the spontaneous emission rate Γ to incorporate decay processes [12].

The density matrix now allows us to calculate the expectation value for the dipole moment, which is given by

$$\langle \mathbf{d} \cdot \epsilon \rangle = d(\rho_{12} + \rho_{21}) = d\left(\sigma_{12} e^{i(\theta+\omega t)} + \sigma_{21} e^{-i(\theta+\omega t)}\right). \tag{17}$$

With this expression and again utilizing the Rotating Wave Approximation, we get from equations (3) and (4) the force

$$\mathbf{F} = \frac{d}{2}\left(\sigma_{12} + \sigma_{21} - i(\sigma_{12} - \sigma_{21})\right) = \frac{\hbar}{2}(U\nabla\Omega + V\Omega\nabla\theta), \tag{18}$$

where we have introduced the notation $U = \sigma_{12} + \sigma_{21}$ and $V = i(\sigma_{12} - \sigma_{21})$, and used the fact that $\dot{\theta} = \nabla\theta(\mathbf{r}) \cdot \dot{\mathbf{r}}$. If the atomic motion is slow, such that the phase of the atomic state, $\dot{\theta}$, does not change much during the lifetime $1/\Gamma$ of the excited state, we can restrict ourselves to the steady-state solution of the density matrix and put the time derivatives of the left side equal to zero in equations (14)–(16). The solutions for the corresponding U and V are then

$$U = \frac{\delta}{\Omega}\frac{s}{s+1} \tag{19}$$

$$V = \frac{\Gamma}{2\Omega}\frac{s}{s+1}, \tag{20}$$

where s is the saturation parameter

$$s = \frac{\Omega^2/2}{(\delta + \dot{\theta})^2 + \Gamma^2/4}. \tag{21}$$

The force acting upon the atom now consists of two parts—the dipole force and the radiation force, respectively,

$$\mathbf{F} = \mathbf{F}_{\text{dip}} + \mathbf{F}_{\text{pr}}, \tag{22}$$

with

$$\mathbf{F}_{\text{dip}} = -\frac{\hbar(\delta + \dot{\theta})}{2} \frac{\nabla s}{s+1}, \tag{23}$$

$$\mathbf{F}_{\text{pr}} = -\frac{\hbar\Gamma}{2} \frac{s}{s+1} \nabla\theta. \tag{24}$$

In the case of plane waves, the latter radiation force $\mathbf{F}_{\text{pr}}$, often referred to as the radiation pressure, is proportional to the wave vector $\mathbf{k} = \nabla\theta$. For trapping purposes, on the other hand, the former dipole force $\mathbf{F}_{\text{dip}}$ is more important. The force $\mathbf{F}_{\text{dip}}$ is determined by the intensity of the laser field. If $s \ll 1$ and $|\delta| \gg \Gamma, \Omega$, we get the corresponding potential using $\mathbf{F}_{\text{dip}} = \nabla W$

$$W = \frac{\hbar\Omega^2}{4\delta} = \frac{d^2E^2}{4\delta\hbar}. \tag{25}$$

From this expression, we can see that if the intensity of the light is inhomogeneous, we obtain a nonzero force whose direction depends upon the sign of the detuning. For a focused Gaussian beam, this means that the atoms are attracted to the high intensity if the laser is red-detuned ($\delta < 0$), i.e., the atoms are the high field seekers. On the other hand, if the laser is blue-detuned ($\delta > 0$), the atoms are the low field seekers and are repelled from the center of the beam.

12.3 THE QUANTUM GAS: BOSE–EINSTEIN CONDENSATES

During recent decades, experimental techniques for trapping and cooling atoms have developed enormously. Experimentalist reached a major goal in 1995 when they were able to trap and cool atomic gases of ^{87}Rb [13], ^{23}Na [14] and ^{7}Li [15] to temperatures low enough to see striking effects of the quantum nature of these gases. The atomic Bose–Einstein condensate (BEC) was born. This literally opened the floodgates in terms of experimental and theoretical activity. One of the main advantages with ultracold atomic quantum gases of either bosons or fermions is the unprecedented possibility to change and manipulate the physical parameters such as density

of the cloud, geometry, or even the interaction strength between the atoms [16]. In addition, the underlying theory describing these gases is remarkably accurate, which have resulted in a very fruitful coexistence between theory and experiments. In this brief introduction to quantum gases, we will give an overview of the basic concepts. In particular, we will concentrate on the theoretical tools we possess and need in order to describe these systems.

12.3.1 Bose–Einstein Condensation in a Cloud of Atoms

There are two types of particles in Nature: *Bosons* which have an integer spin, and *fermions* which have a half integer spin associated with them. Bosons are governed by a symmetric multiparticle wave function and are allowed to all occupy the same quantum state. Fermions, on the other hand, obey the Pauli exclusion principle, which tells us that there cannot be two or more fermions in the same quantum state. The original idea of Bose–Einstein condensation dates back to 1924, when S.N. Bose and A. Einstein were working on a statistical description of light [17,18]. They were able to show that there is a phase transition in a gas of noninteracting particles, where a "condensation" of particles into the lowest state takes place as a consequence of quantum statistical effects. Much later, this phenomenon drew renewed interest in the context of superfluidity when in 1938 F. London predicted that the origin of superfluidity was in Bose–Einstein condensation [19].

Experimental techniques to trap and cool atoms where developed much later. Experimentalists made big advances in the late 1970s when they developed new techniques that used laser cooling and magnetic trapping. The obvious candidate had so far been hydrogen, since it is a light atom with consequently a relatively high critical temperature [20]

$$T_c \sim \frac{\hbar^2 \rho^{2/3}}{m k_B}, \tag{26}$$

where k_B is the Boltzmann constant, m is the mass of the atom, and ρ is the density. Highly sophisticated methods were developed for cooling hydrogen [21], which fortunately paved the way for future experiments. However, it turned out to be surprisingly difficult to reach the quantum regime, which requires high densities in combination with low temperatures. In the 1980s, another candidate(s) entered the scene. Neutral alkali atoms turned out to be well suited for laser cooling and trapping. This is because alkali atoms have suitable level structures and optical transitions that can be addressed with available lasers. Eventually, using a combination of laser cooling and trapping, weak magnetic trapping based upon the Zeeman shift, and evaporative cooling, the experimental groups of Cornell and Wieman at Boulder, Colorado, and Wolfgang Ket-

terle at MIT succeeded in reaching the required high densities and low temperatures for Bose–Einstein condensation. In these two experiments, ^{87}Rb and ^{23}Na were used.

With these experiments, a completely new physical system had been created and now had to be understood. The atomic cloud was trapped, which meant that the condensation did not only take place in momentum space, as it had been traditionally looked at in homogeneous systems, but also in coordinate space. This was new and has resulted in numerous remarkable experiments by groups all over the world where the Bose–Einstein condensate phenomenon is observed in a direct way simply by looking at the density of the cloud and its dynamics.

12.3.2 The Condensate and Its Description

A Bose–Einstein condensate can be understood as a macroscopically occupied single quantum state. We will now look at the weakly interacting gas. The phase transition describing the onset of BEC can be considered using an ideal gas, where the critical temperature is readily derived (see any undergraduate textbook on statistical mechanics [20]). In the following, we will assume zero temperature. This is indeed a legitimate approximation. Present cooling techniques allow the experimentalist to go far below the critical temperature. This is typically in the micro Kelvin regime, where any contribution from the remaining thermal component can be neglected in most cases, as shown in Figure 12.2.

For a dilute gas, only two-body collisions take place. In addition, we obviously have a cold gas, hence we consider only s-wave scattering as the mechanism for the interaction. The interaction potential is therefore of the form [20]

$$V_{\text{int}}(\mathbf{r}-\mathbf{r}') = \frac{4\pi\hbar^2 a}{m}\delta(\mathbf{r}-\mathbf{r}'), \tag{27}$$

where the interaction is described by the single parameter a, called the s-wave scattering length. This is a result of the cold collisions in the gas. For a derivation of equation (27), we have to solve the two-body scattering problem in the limit of zero momentum.

With these assumptions, we get a Hamiltonian of the form

$$\hat{H} = \int d\mathbf{r}\left\{\hat{\Psi}^\dagger(\mathbf{r})\left[-\frac{\hbar^2}{2m}\nabla^2 + V_{\text{ext}}\right]\hat{\Psi}(\mathbf{r}) + \frac{g}{2}\hat{\Psi}^\dagger(\mathbf{r})\hat{\Psi}^\dagger(\mathbf{r})\hat{\Psi}(\mathbf{r})\hat{\Psi}(\mathbf{r})\right\}, \tag{28}$$

where $g = 4\pi\hbar^2 a/m$. As such, this is rather intractable and we have to succumb to approximations. The field operators $\Psi(\mathbf{r},t)$ and $\Psi^\dagger(\mathbf{r},t)$ destroy and creates, respectively, a particle at $\mathbf{r}$ at time t, and obey the usual bosonic commutation rules

$$\left[\hat{\Psi}(\mathbf{r}), \hat{\Psi}^\dagger(\mathbf{r}')\right] = \delta(\mathbf{r}-\mathbf{r}') \tag{29}$$

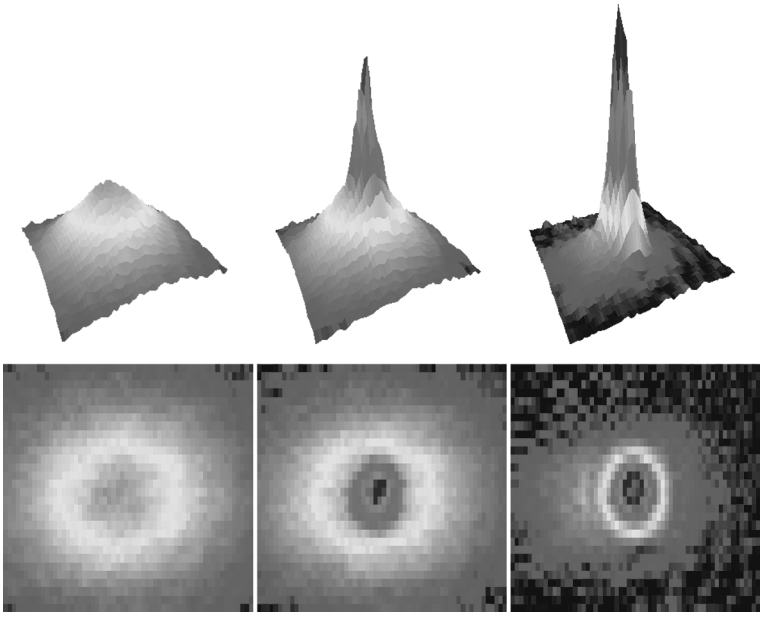

Figure 12.2 The onset of BEC is seen as a sharp peak in the density in the center of the trap. In the figures, the temperature is lowered from left to right. To the far right, we see a pure condensate with a negligible thermal component. The pictures are from the BEC experiment at University of Strathclyde, Glasgow, UK [22]. See color insert.

and

$$\left[\hat{\Psi}(\mathbf{r},t),\hat{\Psi}(\mathbf{r}',t)\right]=\left[\hat{\Psi}^{\dagger}(\mathbf{r},t),\hat{\Psi}^{\dagger}(\mathbf{r}',t)\right]=0. \tag{30}$$

Using these commutation rules, we obtain the Heisenberg equation of motion for the field operator

$$i\hbar\frac{\partial}{\partial t}\hat{\Psi}=[\hat{H},\hat{\Psi}]=-\frac{\hbar^2}{2m}\nabla^2\hat{\Psi}+V_{\text{ext}}(r)\hat{\Psi}+g\hat{\Psi}^{\dagger}\hat{\Psi}\hat{\Psi}. \tag{31}$$

We now split the field operator into the operator for a lowest mode and a part representing the fluctuations and thermal excitations,

$$\hat{\Psi}(\mathbf{r})=\hat{\Psi}_0(\mathbf{r})+\delta\hat{\Psi}(\mathbf{r}). \tag{32}$$

At zero temperature, we can as a first approximation neglect the term standing for the fluctuations $\delta\hat{\Psi}(\mathbf{r})$. In the presence of a condensate, the lowest mode is macroscopically populated, so we can write

$$\hat{\Psi}(\mathbf{r})=\Psi(\mathbf{r})\hat{a}_0\approx\Psi(\mathbf{r})\sqrt{N}. \tag{33}$$

Here we have replaced the annihilation operator $\hat{a}_0$ by $\sqrt{N}$, which is often referred to the Bogoliubov approximation (see, for instance, [4]). This is a legitimate approximation provided the number of atoms N in the condensate is sufficiently large. In other words, we have replaced the field operator by its average

$$\hat{\Psi}(\mathbf{r}) \approx \langle \hat{\Psi}(\mathbf{r}) \rangle = \Psi(\mathbf{r})\sqrt{N}. \tag{34}$$

The resulting equation of motion for the condensate "wavefunction" $\Psi(\mathbf{r})$ then becomes

$$i\hbar \frac{\partial}{\partial t}\Psi(\mathbf{r},t) = \left[-\frac{\hbar^2}{2m}\nabla^2 + V_{\text{ext}}(\mathbf{r}) + g\left|\Psi(\mathbf{r},t)\right|^2\right]\Psi(\mathbf{r},t). \tag{35}$$

This is the celebrated Gross–Pitaevskii equation [4,3]. It is the true workhorse when describing the dynamics of a Bose–Einstein condensate. The Gross–Pitaevskii equation is based on mean field theory, in which each atom feels the presence of all the other atoms through the effective potential. The potential is proportional to the density of the cloud, providing the nonlinear behavior of the condensate. The Gross–Pitaevskii equation is a very useful tool and has been used extensively to describe the properties of Bose–Einstein condensates.

The time-independent version of equation (35) is readily achieved by taking the Ansatz $\Psi(\mathbf{r},t) = \varphi(\mathbf{r})e^{-i\mu t\hbar}$, where μ is the chemical potential

$$\mu\varphi(\mathbf{r}) = \left[-\frac{\hbar^2}{2m}\nabla^2 + V_{\text{ext}}(\mathbf{r}) + g\left|\varphi(\mathbf{r})\right|^2\right]\varphi(\mathbf{r}). \tag{36}$$

A typical density distribution is shown in Figure 12.4, where the atoms are trapped in a harmonic external potential. Due to the interactions between the atoms, the density is not Gaussian, but is closer to an inverse parabola. This can be understood in terms of the Thomas–Fermi approximation [23] which neglects the kinetic energy term in the time-independent Gross–Pitaevskii equation (36) and gives

$$\left|\varphi(\mathbf{r})\right|^2 = \left[\mu - V_{\text{ext}}(\mathbf{r})\right]/g. \tag{37}$$

For harmonic traps, the Thomas–Fermi approximation does indeed give the shape of an inverse parabola for the atomic density shown in Figure 12.4. The approximation works well for trapping frequencies $\omega_z \ll \mu/\hbar$, and only at the edge of the cloud it inevitably breaks down.

12.3.3 Phase Imprinting the Quantum Gas

The trapping of a quantum gas can be achieved by a far detuned laser beam, as shown in the previous section, where the absorption of the light is avoided. With this

technique, it is possible to shape the density of the Bose–Einstein condensate if we can shape the intensity of the light beam. The optical trap does not, however, affect the phase of the quantum gas, which is well defined for every atom in the coherent Bose–Einstein condensate. In order to be able to shape not only the density but also the phase of the Bose–Einstein condensate, we can use the so-called *phase imprinting technique*, which relies on a dynamic process, in contrast to the static optical trap.

The method of phase imprinting consists of passing a short off-resonant laser pulse through an appropriately designed absorption plate or spatial light modulator, which alters the intensity profile of the light beam [24,25]. The shaped light pulse is then allowed to propagate through the Bose–Einstein condensate. In the following, we will illustrate the mechanism by looking at a one-dimensional cloud.

The trapped Bose–Einstein condensate can be considered dynamically one-dimensional if the radial trapping frequency is larger than the corresponding chemical potential, $\omega_r \ll \mu/\hbar$, and the longitudinal confinement of atoms in the trapping potential is much weaker than that in the transverse direction. The Gross–Pitaevskii equation then takes the form

$$i\hbar\frac{\partial}{\partial t}\Psi(z,t) = \left[-\frac{\hbar^2}{2m}\frac{\partial^2}{\partial z^2} + V(z) + W(z,t) + g_{1\mathrm{D}}\left|\Psi(z,t)\right|^2\right]\Psi(z,t), \tag{38}$$

where $W(z,t)$ describes the interaction with the external laser, i.e., the dipole potential generated by the far-detuned laser pulse. The static trapping potential is given by the potential $V(z)$ which is typically harmonic in z. The one-dimensional dynamics is ensured with a renormalized mean field strength,

$$g_{1\mathrm{D}} = g\frac{m\omega_r}{2\pi\hbar}, \tag{39}$$

where ω_r is the transverse trapping frequency. It is important to remember that the dynamics can indeed be one-dimensional, but the collisions are three-dimensional. A true one-dimensional scenario can be achieved by a combination of strong transversal confinement and a low density of the bosonic gas. This phenomenon has been studied extensively both theoretically and experimentally, and is related to a phenomenon where the bosonic gas gets fermionic properties [26].

If the duration of the far off-resonant laser pulse is short compared to the correlation time,

$$t_{\mathrm{corr}} = \frac{\hbar}{\mu}, \tag{40}$$

the condensate does not have time to react, so the dominating term in the right side of equation (38) is given by $W(z,t)$. Consequently, we can write the solution of equation

(38) after the pulse has passed through the condensate as

$$\Psi(z) = e^{-i\int dt' W(z,t')}\Psi_0(z, t=0), \tag{41}$$

where $\Psi_0(z, t=0)$ is the initial state of the condensate. If the incident pulse is sufficiently short, we can extend the integration over time to infinity, hence the acquired phase is given by

$$\phi(z) = \Delta t\, W(z), \tag{42}$$

where Δt is a measure of the width of the pulse in the time domain. The potential $W(z)$ is, as in the case of the optical trap, given by equation (25), so the acquired phase $\phi(z)$ depends on the intensity of the pulse and its duration. In other words, the phase imprinting relies on the timing and shaping of the light beam intensity.

The phase imprinting technique offers a versatile tool for preparing a Bose–Einstein condensate in some chosen state. Generally the prepared state is not an eigenstate of the trapped quantum gas. Consequently, the phase imprinting can be exploited to induce coherent dynamics of the Bose–Einstein condensate. This effect was used when creating dark solitons in Bose–Einstein condensates [24,25]. A *soliton* is a topological excitation, or kink in the wave function, which propagates in the atomic cloud without losing its shape. The soliton is also a particular solution of the nonlinear Gross–Pitaevskii equation. Admittedly, the imprinted state is not the exact soliton solution. But it is close. The phase imprinting procedure therefore does indeed produce dark solitons, i.e., a density notch, in the case of repulsive interactions between the atoms. We are, of course, not restricted to only soliton dynamics. By choosing, for instance, a phase that has a quadratic dependence on position, we can induce focusing or defocusing. Similarly, a linear dependence in position will induce a momentum kick to the gas, which can be used as a method to coherently split a condensate. This is shown in Figures 12.3 and 12.5.

Interestingly, there is a close analogy between optics and the phase imprinting on a Bose–Einstein condensate that acts as a phase plate for the atoms. This is most clearly seen in the focusing dynamics of the cloud of atoms when a parabolically shaped phase is imprinted onto the atoms. Such a phase acts as a lens for the atoms. The focused matter wave, i.e., the condensate, does not, however, focus to a single point later in time due to the interactions between the atoms, but the overall dynamics closely resemble the focusing of light [27,28].

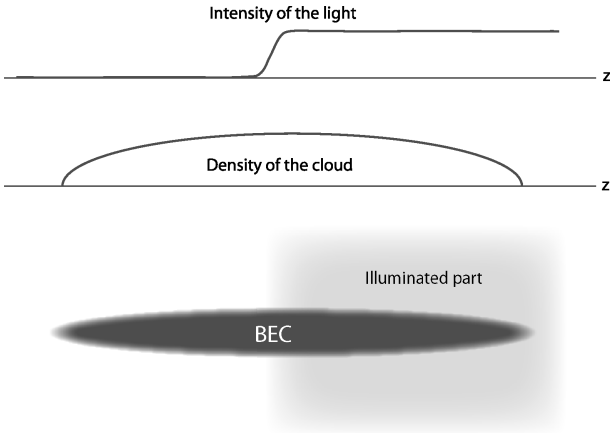

Figure 12.3 The phase imprinting technique can for instance be used for engineering a Bose–Einstein condensate with a sharp phase slip. The resulting dynamics will give rise to dark solitons in the case of repulsive interaction between the atoms.

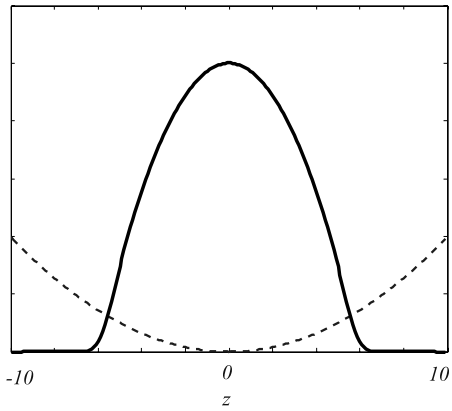

Figure 12.4 The density of the Bose–Einstein condensate has a parabolic shape for $\hbar\omega_z \ll \mu$. The dashed curve indicates the harmonic external trap, $\frac{1}{2}m\omega_z^2 z^2$.

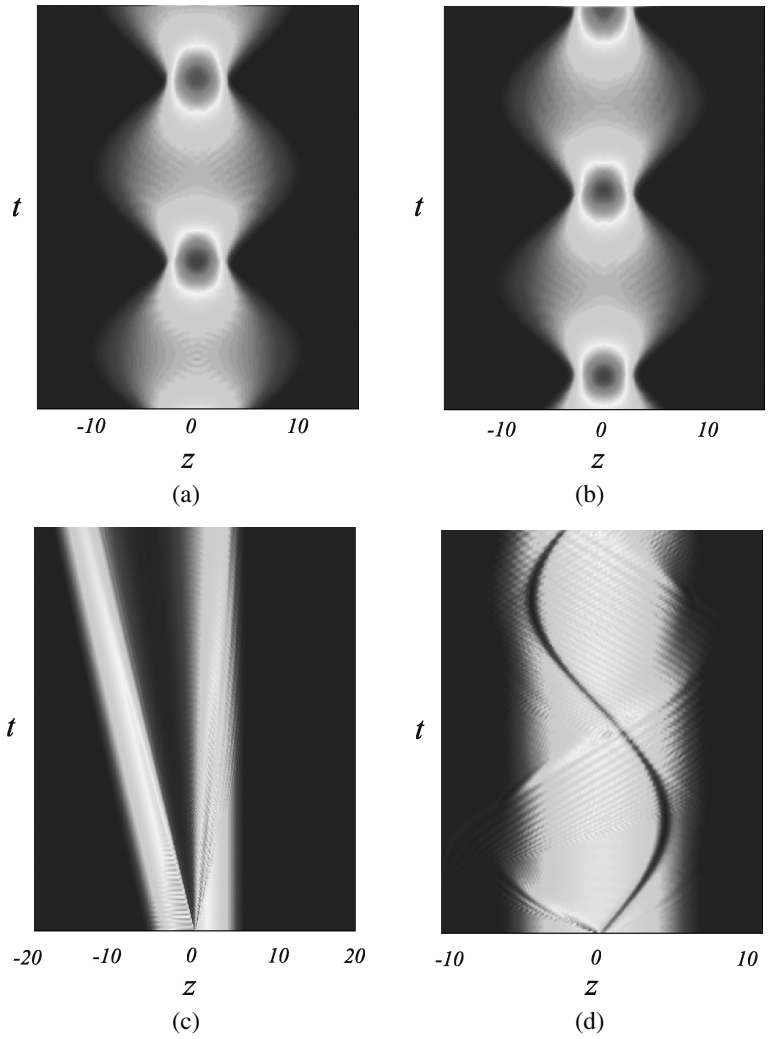

Figure 12.5 The condensate is situated in a harmonic trap. (a) and (b) An imprinted phase that is quadratic in z induces defocusing or focusing, depending upon the sign of the phase gradient. (c) If the phase is chosen such that it is zero for $z > 0$ and linear in z for $z < 0$, the result is a splitting of the cloud where part of the cloud is separated and the remaining part stays stationary during a time much smaller than $1/\omega_z$. (d) With a sharp phase slip imprinted, the result is a dark soliton that oscillates in the cloud (see Figure 12.3). See color insert.

12.4 LIGHT-INDUCED GAUGE POTENTIALS FOR COLD ATOMS

12.4.1 Background

Up to now we have shown that the shaped intensity of the light beam can be used for trapping and phase imprinting a Bose–Einstein condensate. The phase of the light has not played a significant role so far. In this section, we will consider a situation where both the intensity and the phase of the incident laser fields are important in the optical manipulation of atoms. Specifically, we will show how two or more laser fields can induce effective vector and trapping potentials for the atomic center of mass motion. This will give us a new tool for manipulating the neutral atoms because of an induced effective magnetic field. For this, the laser beams should act on the atoms in an Electromagnetically Induced Transparency (EIT) [29–33] configuration. The induced gauge potential has a geometric nature and depends upon the relative intensity and the relative phase of the incident laser fields rather than on their absolute intensities and phases. The technique provides a way to optically induce an effective magnetic field acting on electrically neutral atoms. This happens if the applied laser fields have a nontrivial topology, e.g., if they carry an orbital angular momentum along the propagation direction [5–7,34,35]. The appearance of the effective vector potential is a manifestation of the Mead–Berry connection [36,37] which is encountered in many different areas of physics [38–43].

In passing, we note that the usual way to produce an effective magnetic field in a cloud of electrically neutral atoms is to rotate the system such that the vector potential will appear in the rotating frame of references [44–46]. This would correspond to a situation where the atoms feel a uniform magnetic field. Yet stirring an ultracold cloud of atoms in a controlled manner is a rather demanding task. There have also been suggestions to take advantage of a discrete periodic structure of an optical lattice to introduce asymmetric atomic transitions between the lattice sites [47–50]. Using this approach, one can induce a nonvanishing phase for the atoms moving along a closed path on the lattice, i.e., one can simulate a magnetic flux [51,47–50]. However, such a way of creating the effective magnetic field is inapplicable to an atomic gas that does not constitute a lattice. The light-induced gauge potentials are free from all these drawbacks [5–7,34,52,53]. Furthermore, using these techniques it is possible to induce not only the usual (Abelian) gauge potentials [5–7,34,42,43,53], but also non-Abelian gauge potentials [52,54], whose Cartesian components do not commute. This will be considered in detail in subsequent sections.

12.4.2 General Formalism for the Adiabatic Motion of Atoms in Light Fields

We will start by adapting the general theory of the adiabatic dynamics [36–40] to the center of mass motion of atoms in stationary laser fields. For this we consider atoms with multiple internal states. The full atomic Hamiltonian is

$$\hat{H} = \frac{\hat{p}^2}{2m} + \hat{H}_0(\mathbf{r}) + \hat{V}(\mathbf{r}), \tag{43}$$

where $\hat{\mathbf{p}} \equiv -i\hbar\nabla$ is the momentum operator for an atom positioned at $\mathbf{r}$, and m is the atomic mass. Here the Hamiltonian $\hat{H}_0(\mathbf{r})$ describes the electronic degrees of freedom of the atom, and $\hat{V}(\mathbf{r})$ represents an external trapping potential. Note that the atomic Hamiltonian $\hat{H}_0(\mathbf{r})$ accommodates effects due to external light fields in addition to the internal dynamics.

For a fixed position $\mathbf{r}$, the atomic Hamiltonian $\hat{H}_0(\mathbf{r})$ can be diagonalized to give a set of, say, N dressed states $|\chi_n(\mathbf{r})\rangle$ of the atom coupled with the light fields. The dressed states are characterized by eigenvalues $\varepsilon_n(\mathbf{r})$, with $n = 1, 2, \ldots, N$. The full quantum state of the atom describing both internal and motional degrees of freedom can then be expanded in terms of the dressed states as

$$|\Phi\rangle = \sum_{n=1}^{N} \Psi_n(\mathbf{r})\big|\chi_n(\mathbf{r})\big\rangle, \tag{44}$$

where $\Psi_n(\mathbf{r}) \equiv \Psi_n$ is a wave-function for the center of mass motion of the atom in the internal state n. Substituting equation (44) into the Schrödinger equation $i\hbar\partial|\Phi\rangle/\partial t = \hat{H}|\Phi\rangle$, one arrives at a set of coupled equations for the components Ψ_n. Introducing the N-dimensional column vector $\Psi = (\Psi_1, \Psi_2, \ldots, \Psi_N)^T$, it is convenient to represent these equations in a matrix form,

$$i\hbar\frac{\partial}{\partial t}\Psi = \left[\frac{1}{2m}(-i\hbar\nabla - \mathbf{A})^2 + U\right]\Psi, \tag{45}$$

where $\mathbf{A}$ and U are $N \times N$ matrices with the following elements

$$\mathbf{A}_{n,m} = i\hbar\big\langle\chi_n(\mathbf{r})\big|\nabla\chi_m(\mathbf{r})\big\rangle, \tag{46}$$

$$U_{n,m} = \varepsilon_n(\mathbf{r})\delta_{n,m} + \big\langle\chi_n(\mathbf{r})\big|\hat{V}(\mathbf{r})\big|\chi_m(\mathbf{r})\big\rangle. \tag{47}$$

The latter matrix U includes contributions from both the internal atomic energies and also the external trapping potential. The former matrix $\mathbf{A}$ is the gauge potential that appears due to the position dependence of the atomic dressed states. If the off-diagonal elements of the matrices $\mathbf{A}$ and U are much smaller than the difference in the atomic energies $U_{nn} - U_{mm}$, the *adiabatic approximation* can be applied by neglecting the

off-diagonal contributions. This leads to a separation of the dynamics in different dressed states. Atoms in any one of the dressed states evolve according to a separate Hamiltonian in which the gauge potential $\mathbf{A}$ reduces to the 1×1 matrix, i.e., the gauge potential becomes Abelian. The adiabatic approximation fails if there are degenerate (or nearly degenerate) dressed states, so that the off-diagonal (nonadiabatic) couplings between the degenerate dressed states can no longer be ignored. In that case, the gauge potentials no longer reduce to the 1×1 matrices. They are non-Abelian provided their Cartesian components do not commute.

Let us assume that the first q atomic dressed states are degenerate (or nearly degenerate) and that these levels are well separated from the remaining $N - q$ levels. Neglecting transitions to the remaining states, one can project the full Hamiltonian onto this subspace. As a result, one arrives at the closed Schrödinger equation for the reduced column vector $\tilde{\Psi} = (\Psi_1, \ldots, \Psi_q)^\top$

$$i\hbar \frac{\partial}{\partial t}\tilde{\Psi} = \left[\frac{1}{2m}(-i\hbar\nabla - \mathbf{A})^2 + U + \Phi\right]\tilde{\Psi}, \tag{48}$$

where $\mathbf{A}$ and U are the truncated $q \times q$ matrices. The projection of the term $\mathbf{A}^2$ to the q-dimensional subspace cannot entirely be expressed in terms of a truncated matrix $\mathbf{A}$. This gives rise to a geometric scalar potential Φ, which is again a $q \times q$ matrix,

$$\begin{aligned}\Phi_{n,m} &= \frac{1}{2m}\sum_{l=q+1}^{N} \mathbf{A}_{n,l} \cdot \mathbf{A}_{l,m} \\ &= \frac{\hbar^2}{2m}\left(\langle\nabla\chi_n|\nabla\chi_m\rangle + \sum_{k=1}^{q}\langle\chi_n|\nabla\chi_k\rangle\langle\chi_k|\nabla\chi_m\rangle\right),\end{aligned} \tag{49}$$

with $n, m \in (1, \ldots, q)$. The reduced $q \times q$ matrix $\mathbf{A}$ is the Mead–Berry connection [36,37], also known as the effective *vector potential*. It is related to a curvature (an effective "magnetic" field) $\mathbf{B}$ as

$$B_i = \frac{1}{2}\epsilon_{ikl}F_{kl}, \quad F_{kl} = \partial_k A_l - \partial_l A_k - \frac{i}{\hbar}[A_k, A_l]. \tag{50}$$

Note that the term $\frac{1}{2}\varepsilon_{ikl}[A_k, A_l] = (\mathbf{A} \times \mathbf{A})_i$ does not vanish in general because the vector components of $\mathbf{A}$ do not necessarily commute. In fact this term reflects the non-Abelian character of the gauge potentials.

In the next section, we will consider a situation where two laser beams are coupled to the atoms in the so-called Λ *configuration*. In this scheme, there is a single nondegenerate electronic state (known as a *dark state*). Thus, the atomic center of mass undergoes the adiabatic motion influenced by the (Abelian) vector and trapping potentials. Later in the chapter, we will analyze a tripod scheme of laser–atom inter-

actions that provides two degenerate dark states. In that case, one has non-Abelian light-induced gauge potentials.

12.5 LIGHT-INDUCED GAUGE POTENTIALS FOR THE Λ SCHEME

12.5.1 General

We will now consider an ensemble of cold three-level atoms in the Λ configuration with two ground states $|1\rangle$ and $|2\rangle$ and an electronically excited state $|0\rangle$, as shown in Figure 12.6. For example, the states $|1\rangle$ and $|2\rangle$ can be different hyperfine ground states of an atom. The atoms interact with two resonant laser beams in the EIT configuration, as shown in Figure 12.6. The first beam has a frequency of ω_1 and a wave-vector of $\mathbf{k}_1$, and it induces the atomic transitions $|1\rangle \rightarrow |0\rangle$ with Rabi frequency $\Omega_1 \equiv \mu_{01} E_1/2$, where E_1 is the electric field strength and μ_{01} is the dipole moment for the transition from the ground state $|1\rangle$ to the excited state $|0\rangle$. The second beam is characterized by the frequency ω_2 and wave-vector $\mathbf{k}_2$. It causes the transition $|2\rangle \rightarrow |0\rangle$ with a Rabi frequency $\Omega_2 \equiv \mu_{02} E_2/2$.

When adopting the rotating wave approximation, the Hamiltonian for the electronic degrees of freedom of an atom interacting with the two beams becomes

$$\hat{H}_0(\mathbf{r}) = \epsilon_{21}|2\rangle\langle 2| + \epsilon_{01}|0\rangle\langle 0| - \hbar\big(\Omega_1|0\rangle\langle 1| + \Omega_2|0\rangle\langle 2| + \text{H.c.}\big), \tag{51}$$

where ϵ_{21} and ϵ_{01} are, respectively, the energies of the detuning from the two- and single-photon resonances. Note that the spatial dependence of the Hamiltonian $\hat{H}_0(\mathbf{r})$ emerges through the spatial dependence of the Rabi frequencies $\Omega_1 \equiv \Omega_1(\mathbf{r})$ and $\Omega_2 \equiv \Omega_2(\mathbf{r})$.

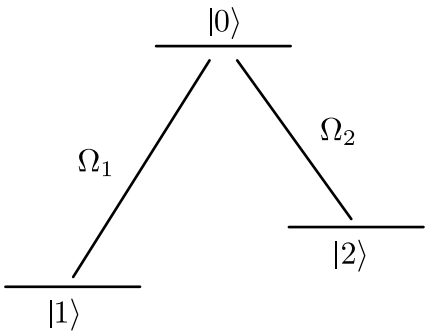

Figure 12.6 The EIT Λ configuration with two laser beams Ω_1 and Ω_2 coupling the levels.

Neglecting the two-photon detuning ($\epsilon_{21} = 0$), the Hamiltonian (51) has the eigenstate

$$|D\rangle = \frac{1}{\sqrt{1+|\zeta|^2}}\big(|1\rangle - \zeta|2\rangle\big), \tag{52}$$

representing a coherent superposition of both ground states, where

$$\zeta = \frac{\Omega_1}{\Omega_2} \tag{53}$$

is the ratio of the amplitudes of the laser fields. It is characterized by a zero eigenenergy: $\hat{H}_0(\mathbf{r})|D\rangle = 0$. Since the state $|D\rangle$ has no contribution from the excited electronic state $|0\rangle$ and is not coupled to that state, it is immune to absorption and spontaneous emission. Therefore, the state $|D\rangle$ is called the dark state [29–33]. We are interested in a situation where the atoms are kept in their dark state $|D\rangle \equiv |D(\mathbf{r})\rangle$, so that the full atomic state-vector is

$$|\Phi\rangle = \Psi_D(\mathbf{r})\big|D(\mathbf{r})\big\rangle, \tag{54}$$

where Ψ_D is the wave-function for the center of mass motion of the dark-state atoms. If an atom is in the dark state $|D\rangle$, the laser beams induce the absorption paths $|2\rangle \to |0\rangle$ and $|1\rangle \to |0\rangle$, which interfere destructively, resulting in the Electromagnetically Induced Transparency [29–33]. In such a situation, the transitions to the upper atomic level $|0\rangle$ are suppressed. That is why the dark state has no contribution by the excited electronic state $|0\rangle$.

Suppose once again that the laser fields are tuned to the two-photon resonance: $\epsilon_{21} = 0$. The remaining two photon mismatch (if any) can be accommodated within the trapping potential

$$\hat{V}(\mathbf{r}) = V_1(\mathbf{r})|1\rangle\langle 1| + V_2(\mathbf{r})|2\rangle\langle 2| + V_0(\mathbf{r})|0\rangle\langle 0|, \tag{55}$$

where $V_j(\mathbf{r})$ is the trapping potential for an atom in the electronic state j, with $j = 0, 1, 2$. Applying the treatment presented in the previous section, the center of mass dynamics of the dark-state atoms is described by the equation of motion

$$i\hbar\frac{\partial}{\partial t}\Psi_D = \left[\frac{1}{2m}(-i\hbar\nabla - \mathbf{A})^2 + V_{\text{eff}}\right]\Psi_D, \tag{56}$$

where $\mathbf{A}$ and V_{eff} are the effective vector and trapping potentials, respectively,

$$\mathbf{A} = i\hbar\langle D|\nabla D\rangle, \tag{57}$$

$$V_{\text{eff}} = V + \phi, \tag{58}$$

with

$$V = \frac{V_1(\mathbf{r}) + |\zeta|^2 V_2(\mathbf{r})}{1 + |\zeta|^2}, \tag{59}$$

$$\phi = \frac{\hbar^2}{2M}\big(\langle D|\nabla D\rangle^2 + \langle \nabla D|\nabla D\rangle\big). \tag{60}$$

Since $V_1(\mathbf{r})$ and $V_2(\mathbf{r})$ are the trapping potentials for an atom in the electronic states 1 and 2, the potential V represents the external trapping potential for an atom in the dark state.

In this way, the effective trapping potential V_{eff} is composed of the external trapping potential V and the geometric scalar potential ϕ. The former V is determined by the shape of the trapping potentials $V_1(\mathbf{r})$ and $V_2(\mathbf{r})$, as well as the intensity ratio $|\zeta|^2$. The latter geometric potential ϕ is determined exclusively by the spatial dependence of the dark state $|D\rangle$ emerging through the spatial dependence of the ratio of the Rabi frequencies $\zeta = \Omega_1/\Omega_2$. Note that the effective vector potential $\mathbf{A}$ has a geometric nature as well because it also originates from the spatial dependence of the dark state.

12.5.2 Adiabatic Condition

The separation between the energies of the dark state and the remaining dressed atomic states of the Λ system is characterized by the total Rabi frequency $\Omega = \sqrt{\Omega_1^2 + \Omega_2^2}$. Assuming that the laser fields are tuned to the one- and two-photon resonances ($\epsilon_{01}, \epsilon_{21} \ll \hbar\Omega$), the adiabatic approach holds if the off-diagonal matrix elements in equation (45) are much smaller than the total Rabi frequency Ω. This leads to the following condition

$$F \ll \Omega, \tag{61}$$

where the velocity-dependent term

$$F = \frac{1}{1 + |\zeta|^2}|\nabla\zeta \cdot \mathbf{v}| \tag{62}$$

reflects the two-photon Doppler detuning. Note that the condition (61) does not accommodate effects due to the decay of the excited atoms. The dissipative effects can be included by replacing the energy of the one-photon detuning ϵ_{01} by $\epsilon_{01} - i\hbar\gamma_0$, where γ_0 is the excited-state decay rate. In such a situation, the dark state can be shown to acquire a finite lifetime

$$\tau_D \sim \gamma_0^{-1}\Omega^2/F^2, \tag{63}$$

which should be large compared to other characteristic times of the system.

The condition (61) implies that the inverse Rabi frequency Ω^{-1} should be smaller than the time an atom travels a characteristic length over which the amplitude or the phase of the ratio $\zeta = \Omega_1/\Omega_2$ changes considerably. The latter length exceeds the optical wavelength, and the Rabi frequency can be of the order of 10^7 to 10^8 s^{-1} [55]. Consequently, the adiabatic condition (61) should hold for atomic velocities up to the order of tens of meters per second, i.e., up to extremely large velocities in the context of ultra-cold atomic gases. The allowed atomic velocities become lower if the spontaneous decay of the excited atoms is taken into account. According to equation (63), the atomic dark state acquires then a finite lifetime τ_D, which is equal to γ_0^{-1} times the ratio Ω^2/F^2. The atomic decay rate γ_3 is typically of the order 10^7 s^{-1}. Therefore, in order to achieve long-lived dark states, the atomic velocity should not be too large. For instance, if the atomic velocities are of the order of a centimeter per second (a typical speed of sound in an atomic BEC), the atoms should survive in their dark states up to a few seconds. This is comparable to the typical lifetime of an atomic BEC.

12.5.3 Effective Vector and Trapping Potentials

Let us express the ratio of Rabi frequencies ζ in terms of amplitude and phase as

$$\zeta = \frac{\Omega_1}{\Omega_2} = |\zeta| e^{iS}. \tag{64}$$

Using expression (52) for the dark state, the effective vector potential takes the form

$$\mathbf{A} = -\hbar \frac{|\zeta|^2}{1+|\zeta|^2} \nabla S. \tag{65}$$

The effective magnetic field is consequently

$$\mathbf{B} = \hbar \frac{\nabla S \times \nabla |\zeta|^2}{(1+|\zeta|^2)^2}, \tag{66}$$

and the geometric scalar potential reads

$$\phi = \frac{\hbar^2}{2M} \frac{(\nabla|\zeta|)^2 + |\zeta|^2 (\nabla S)^2}{(1+|\zeta|^2)^2}. \tag{67}$$

One can easily recognize that the gauge potential $\mathbf{A}$ yields a nonvanishing effective magnetic field $\mathbf{B} = \nabla \times \mathbf{A}$ only if the gradients of the relative intensity and the relative phase are both nonzero and not parallel to each other. Therefore the effective magnetic field cannot be induced using the plane waves for the Λ scheme [42,43]. However,

plane waves can indeed be used in a more complicated tripod setup [52,54], which we will consider in the next section.

Equation (66) has a very intuitive interpretation. Here $\nabla[|\zeta|^2/(1+|\zeta|^2)]$ is a vector that connects the "center of mass" of the two light beams, and ∇S is proportional to the vector of the relative momentum of the two light beams. Thus, a nonvanishing $\mathbf{B}$ requires a *relative orbital angular momentum* of the two light beams. We will see that this is the case for light beams with a vortex [5–7,34] or if one uses two counter-propagating light beams of finite diameter with an axis offset [53].

12.5.4 Co-Propagating Beams with Orbital Angular Momentum

Let us suppose that the incident laser beams can carry an orbital angular momentum along the propagation axis z, as shown in Figure 12.7. In this case, the spatial distribution of the beams is [56,57]

$$\Omega_1 = \Omega_1^{(0)} e^{i(k_1 z + l_1 \phi)} \tag{68}$$

and

$$\Omega_2 = \Omega_2^{(0)} e^{i(k_2 z + l_2 \phi)}, \tag{69}$$

where $\Omega_1^{(0)}$ and $\Omega_2^{(0)}$ are slowly varying amplitudes, $\hbar l_1$ and $\hbar l_2$ are the corresponding orbital angular momenta per photon along the propagation axis z, and ϕ is the azimuthal angle. The phase of the ratio $\zeta = \Omega_1/\Omega_2$ then reads $S = l\phi$. Therefore, the effective vector potential and the magnetic field take the form

$$\mathbf{A} = -\frac{\hbar l}{\rho} \frac{|\zeta|^2}{1+|\zeta|^2} \hat{\mathbf{e}}_\phi, \tag{70}$$

$$\mathbf{B} = \frac{\hbar l}{\rho} \frac{1}{(1+|\zeta|^2)^2} \hat{\mathbf{e}}_\phi \times \nabla |\zeta|^2, \tag{71}$$

where $l = l_1 - l_2$ is the difference in the winding numbers of the laser beams, $\mathbf{e}_\phi$ is the unit vector in the azimuthal direction, and ρ is the cylindrical radius. Note that although both beams are generally allowed to have nonzero orbital angular momentum by equations (68) and (69), it is desirable for the angular momentum to be zero for one of these beams. In fact, if both l_1 and l_2 were nonzero, the amplitudes Ω_1 and Ω_2 would simultaneously go to zero at the origin where $\rho = 0$. In that situation, the

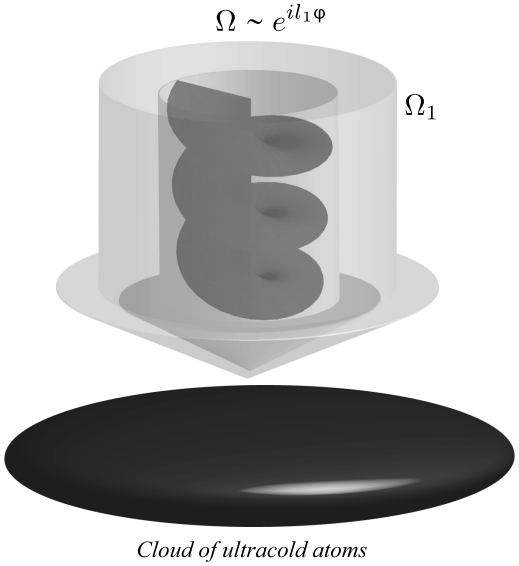

Figure 12.7 At least one of the two coupling beams in the EIT configuration should have an orbital angular momentum. See color insert.

total Rabi frequency $\Omega = \sqrt{\Omega_1^2 + \Omega_2^2}$ would also vanish, leading to the violation of the adiabatic condition (61) at $\rho = 0$.

If the beams are cylindrically symmetric, the intensity ratio $|\zeta|^2$ depends upon the cylindrical radius ρ only. In that case, the effective magnetic field is directed along the z-axis:

$$\mathbf{B} = -\hat{\mathbf{e}}_z \frac{\hbar l}{\rho} \frac{1}{(1+|\zeta|^2)^2} \frac{\partial}{\partial \rho} |\zeta|^2. \tag{72}$$

It is evident that the effective magnetic field is nonzero only if the ratio $\zeta = \Omega_1/\Omega_2$ contains a nonzero phase ($l = l_1 - l_2 \neq 0$) and the amplitude $|\zeta|$ has a radial dependence ($\partial|\zeta|/\partial\rho \neq 0$).

The light-induced magnetic field affects the atomic motion in the xy-plane. This might lead to a number of phenomena, such as the de Haas–van Alphen effect in the cloud of atomic fermions [5], or the light-induced Meissner effect [34] in the atomic Bose–Einstein condensates. Furthermore, the light-induced potentials alter the expansion dynamics of the atomic cloud [35]. A more detailed analysis of the light-induced gauge potentials for this geometry is presented in references [5–7,34].

12.5.5 Counterpropagating Beams with Shifted Transverse Profiles

We will now consider a different scenario [53], where we will use two counterpropagating light beams of finite diameter with an axis offset for which $\Omega_1 = \Omega_1^{(0)} e^{ik_1 y}$ and $\Omega_2 = \Omega_2^{(0)} e^{-ik_2 y}$, where $\Omega_1^{(0)}$ and $\Omega_2^{(0)}$ are real amplitudes with shifted transverse profiles, as shown in Figure 12.8. The beams possess a required relative orbital angular momentum similarly to two point particles with constant momenta passing each other at some finite distance, hence, an effective magnetic field will be generated.

The phase of the ratio $\zeta = \Omega_1/\Omega_2$ is now given by

$$S = ky, \quad k = k_1 + k_2, \tag{73}$$

so that $\nabla S = k\hat{\mathbf{e}}_y$ where $\hat{\mathbf{e}}_y$ is a unit Cartesian vector. The spatial dependence of the intensity ratio $|\zeta|^2 = |\Omega_1/\Omega_2|^2$ is determined by the spatial profiles of both $|\Omega_1|^2$ and $|\Omega_2|^2$. Since the light beams counterpropagate along the y-axis, their intensities depend weakly on the propagation distance y. Furthermore, we shall disregard the z-dependence of the intensity ratio $|\zeta|^2$. This is legitimate, for instance, if the atomic motion is confined to the xy-plane due to a strong trapping potential in the z-direction. Using equation (66), one arrives at the following strength of the light-induced effective magnetic field

$$\mathbf{B} = -\hat{\mathbf{e}}_z \hbar k \frac{\partial}{\partial x} \frac{|\zeta|^2}{(1 + |\zeta|^2)}. \tag{74}$$

The effective magnetic field $\mathbf{B}$ is oriented along the z-axis. Its magnitude B depends generally upon the x-coordinate, yet it has a weak y-dependence as long as the paraxial approximation holds.

One possible application of this technique is to study quantum Hall phenomena and thus the possibility to enter the lowest Landau level (LLL) regime for the trapped atoms. In doing so, we have to estimate the maximum strength of the magnetic field.

Figure 12.8 Two counterpropagating and overlapping laser beams interact with a cloud of cold atoms.

For this we determine the minimum area needed for a magnetic flux to correspond to a single flux quantum $2\pi\hbar$. From equation (74), we recognize that this area is given by the product $\lambda\, x_{\rm eff}$, where $x_{\rm eff}$ is the effective separation between the two beam centers and $\lambda = 4\pi/k$. To reach the LLL in a two-dimensional gas, the atomic density therefore has to be smaller than one atom per $\lambda\, x_{\rm eff}$.

The above analysis holds as long as the atoms move sufficiently slow to remain in their dark states. This is the case if the adiabatic condition given by equation (62) holds. In the present situation, the adiabatic condition takes the form

$$F^2 = \frac{1}{(1+|\zeta|^2)^2}\left[\left(v_x \frac{\partial}{\partial x}|\zeta|\right)^2 + \left(|\zeta| k v_y\right)^2\right] \ll \Omega^2. \tag{75}$$

Let us assume that both beams are characterized by Gaussian profiles with the same amplitude Ω_0 and width σ

$$|\Omega_j| = \Omega_0 \exp\left(-\frac{(x-x_j)^2}{\sigma^2}\right), \quad j = 1, 2. \tag{76}$$

In the paraxial approximation, the Gaussian beams have the width $\sigma \equiv \sigma(y) = \sigma_0[1 + (\lambda y/\pi\sigma_0^2)]^{1/2}$, where $\sigma_0 \equiv \sigma(0)$ is the beam waist and λ is the wavelength. Since $k_1 \approx k_2 \approx k/2$, we have $\lambda \approx 4\pi/k$ for both beams. We are interested mostly in distances $|y|$ much less than the confocal parameter of the beams $b = 2\pi\sigma_0^2/\lambda \approx k\sigma_0^2/2$. For such distances, $|y| \ll b$, the width $\sigma(y)$ is close to the beam waist: $\sigma(y) \approx \sigma_0$.

Suppose the beams are centered at $x_1 = x_0 + \Delta x/2$ and $x_2 = x_0 - \Delta x/2$. The intensity ratio then reads: $|\zeta|^2 \equiv |\Omega_1/\Omega_2|^2 = \exp[(x - x_0)/a]$, where $a \equiv a(y) = \sigma^2/4\Delta x$ is the relative width of the two beams. Thus we have

$$\mathbf{B} = -\hbar k \frac{1}{4a\cosh^2((x-x_0)/2a)}\mathbf{e}_z, \tag{77}$$

$$V_{\rm eff}(\mathbf{r}) = V(\mathbf{r}) + \frac{\hbar^2 k^2}{2m}\frac{(1 + 1/4a^2k^2)}{4\cosh^2((x-x_0)/2a)}, \tag{78}$$

where $V(\mathbf{r})$ is the external trapping potential. It is evident that both $\mathbf{B}$ and $V_{\rm eff}(\mathbf{r})$ are maximum at the central point $x = x_0$ and decrease quadratically for $|x - x_0| \ll a$. The term *quadratic* in the displacement $x - x_0$ can be cancelled out in the effective trapping potential (78) by taking an external potential $V(\mathbf{r})$ containing the appropriate quadratic term. The frequency of the external potential fulfilling such a condition is

$$\omega_{\rm ext} = \frac{\hbar k}{4am}\sqrt{1 + 1/4a^2k^2}. \tag{79}$$

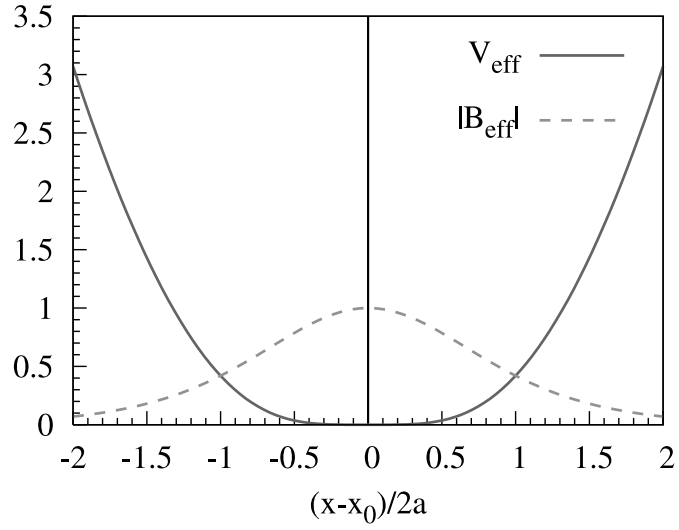

Figure 12.9 Effective trapping potential V_{eff} and effective magnetic field B_{eff} produced by counter-propagating Gaussian beams. The external harmonic potential V_{ext} cancels the quadratic term in the overall potential V_{eff}. The effective magnetic field is plotted in the units of $B(0) \equiv \hbar k/4a$, whereas the effective trapping potential is plotted in the units of $\hbar\omega_{\text{rec}}(1 + 1/4a^2k^2)$, with $\omega_{\text{rec}} = \hbar k^2/2m$.

With this, the overall effective trapping potential becomes constant up to terms of the fourth order in $x - x_0$. In the vicinity of the central point ($|x - x_0| \ll a$), the magnetic field strength is $B \approx \hbar k/4a$. The corresponding magnetic length and cyclotron frequency are $\ell_B \approx \sqrt{\hbar/B} = 2\sqrt{a/k}$ and $\omega_c = B/m \approx \hbar k/4am$. The magnetic length ℓ_B is much smaller than the relative width of the two beams, $\ell_B \ll a$, provided the latter is much larger than the optical wave length, $ak \gg 1$. In that case, many magnetic lengths fit within the interval $|x - x_0| < a$ across the beams. Furthermore, the cyclotron frequency is then approximately equal to the frequency of the external trap: $\omega_c \approx \omega_{\text{ext}}$, both of them being much less than the recoil frequency.

Figure 12.9 shows the effective trapping potential and effective magnetic field calculated using equations (77) and (78), where the external harmonic potential V_{ext} with frequency ω_{ext} (equation (79)) is added to cancel the quadratic term in the overall potential $V(\mathbf{r})$. The magnetic field is seen to be close to its maximum value in the area of constant potential, where $|x - x_0| \ll a$. For larger distances, the effective trapping potential forms a barrier, so the atoms can be trapped in the region of large magnetic field.

12.6 LIGHT-INDUCED GAUGE FIELDS FOR A TRIPOD SCHEME

12.6.1 General

Let us now consider a more complex tripod scheme [52,58] of the atom-light coupling shown in Figure 12.10, in which there is an additional third laser driving the transitions between an extra ground state 3 and the excited state 0. Assuming exact single- and two-photon resonances, the Hamiltonian of the tripod system reads in interaction representation

$$\hat{H}_0 = -\hbar\left(\Omega_1|0\rangle\langle 1| + \Omega_2|0\rangle\langle 2| + \Omega_3|0\rangle\langle 3|\right) + \text{H.c.} \tag{80}$$

The Hamiltonian $\hat{H}_0$ has two eigen-states $|D_j\rangle$ ($j = 1, 2$) characterized by zero eigen-energies $\hat{H}_0|D_j\rangle = 0$. The eigen-states $|D_j\rangle$ are the dark states containing no excited-state contribution, as one can see in equations (82) and (83).

Parameterizing the Rabi-frequencies Ω_μ with angle and phase variables according to

$$\begin{aligned}
\Omega_1 &= \Omega \sin\theta \cos\phi\, e^{iS_1}, \\
\Omega_2 &= \Omega \sin\theta \sin\phi\, e^{iS_2}, \\
\Omega_3 &= \Omega \cos\theta e^{iS_3},
\end{aligned} \tag{81}$$

where $\Omega = \sqrt{|\Omega_1|^2 + |\Omega_2|^2 + |\Omega_3|^2}$, the adiabatic dark states read

$$|D_1\rangle = \sin\phi e^{iS_{31}}|1\rangle - \cos\phi e^{iS_{32}}|2\rangle, \tag{82}$$

$$|D_2\rangle = \cos\theta\cos\phi e^{iS_{31}}|1\rangle + \cos\theta\sin\phi e^{iS_{32}}|2\rangle - \sin\theta|3\rangle, \tag{83}$$

with $S_{ij} = S_i - S_j$ being the relative phases. As in the Λ scheme, the dark states are eigen-states of the Hamiltonian $\hat{H}_0$ with zero eigen-energy: $\hat{H}_0|D_j\rangle = 0$. The dark

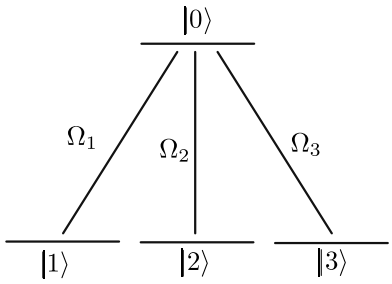

Figure 12.10 The tripod configuration.

states depend upon the atomic position through the spatial dependence of the Rabi-frequencies Ω_j. This leads to the appearance of the gauge potentials $\mathbf{A}$ and Φ considered below.

We are interested in a situation where the atoms are kept in their dark states. This can be done neglecting transitions from the dark states to the bright state $|B\rangle \sim \Omega_1^*|1\rangle + \Omega_2^*|2\rangle + \Omega_3^*|3\rangle$. The latter is coupled to the excited state $|0\rangle$ with the Rabi frequency Ω, so the two states $|B\rangle$ and $|0\rangle$ split into a doublet separated from the dark states by the energies $\pm\Omega$. The adiabatic approximation is justified if Ω is sufficiently large compared to the two-photon detuning due to the laser mismatch and/or Doppler shift. In that case, the internal state of an atom does indeed evolve within the dark state manifold. The atomic state-vector $|\Phi\rangle$ can then be expanded in terms of the dark states according to $|\Phi\rangle = \sum_{j=1}^{2} \Psi_j(\mathbf{r})|D_j(\mathbf{r})\rangle$, where $\Psi_j(\mathbf{r})$ is the wave-function for the center of mass motion of the atom in the jth dark state. Adapting the general treatment used is the section on light-induced gauge potentials for cold atoms, the atomic center of mass motion is described by a two-component wave-function

$$\Psi = \begin{pmatrix} \Psi_1 \\ \Psi_2 \end{pmatrix}, \tag{84}$$

which obeys the Schrödinger equation

$$i\hbar \frac{\partial}{\partial t}\Psi = \left[\frac{1}{2m}(-i\hbar\nabla - \mathbf{A})^2 + V + \Phi\right]\Psi, \tag{85}$$

where the potentials $\mathbf{A}$, Φ, and V are 2×2 matrices. The former $\mathbf{A}$ and Φ are light-induced gauge potentials emerging due to the spatial dependence of the atomic dark states [52]

$$\begin{aligned}
\mathbf{A}_{11} &= \hbar\left(\cos^2\phi\nabla S_{23} + \sin^2\phi\nabla S_{13}\right), \\
\mathbf{A}_{12} &= \hbar\cos\theta\left(\frac{1}{2}\sin(2\phi)\nabla S_{12} - i\nabla\phi\right), \\
\mathbf{A}_{22} &= \hbar\cos^2\theta\left(\cos^2\phi\nabla S_{13} + \sin^2\phi\nabla S_{23}\right),
\end{aligned} \tag{86}$$

and

$$\Phi_{11} = \frac{\hbar^2}{2m}\sin^2\theta\left(\frac{1}{4}\sin^2(2\phi)(\nabla S_{12})^2 + (\nabla\phi)^2\right),$$

$$\Phi_{12} = \frac{\hbar^2}{2m}\sin\theta\left(\frac{1}{2}\sin(2\phi)\nabla S_{12} - i\nabla\phi\right)$$
$$\left(\frac{1}{2}\sin(2\theta)\left(\cos^2\phi\nabla S_{13} + \sin^2\phi\nabla S_{23}\right) - i\nabla\theta\right),$$
$$\Phi_{22} = \frac{\hbar^2}{2m}\left(\frac{1}{4}\sin^2(2\theta)\left(\cos^2\phi\nabla S_{13} + \sin^2\phi\nabla S_{23}\right)^2 + (\nabla\theta)^2\right). \quad (87)$$

Since the level scheme considered in Figure 12.10 corresponds to that of Alkali atoms where $|1\rangle$, $|2\rangle$, and $|3\rangle$ are Zeeman components of hyperfine levels, it is natural to assume that the external trapping potential is diagonal in these states and has the form $V = V_1(\mathbf{r})|1\rangle\langle 1| + V_2(\mathbf{r})|2\rangle\langle 2| + V_3(\mathbf{r})|3\rangle\langle 3|$. This still takes into account the fact that magnetic, magneto-optical, or optical dipole forces can be different or various Zeeman states. According to equation (47), the external potential in the adiabatic basis is then given by a 2×2 matrix with elements $V_{jk} = \langle D_j|V|D_k\rangle$. Using the expressions for the dark states (82) and (83), we arrive at the following matrix elements of the external potential [52]

$$V_{11} = V_2\cos^2\phi + V_1\sin^2\phi,$$
$$V_{12} = \frac{1}{2}(V_1 - V_2)\cos\theta\sin(2\phi),$$
$$V_{22} = \left(V_1\cos^2\phi + V_2\sin^2\phi\right)\cos^2\theta + V_3\sin^2\theta. \quad (88)$$

At this point, it is instructive to consider some specific examples.

12.6.2 The Case where $S_{12} = 0$

Let us first assume that the laser fields that couple the levels $|1\rangle$ and $|2\rangle$ are copropagating and have the same frequency and the same orbital angular momentum (if any). In this case, their relative phase is fixed and can be put to zero $S_{12} = 0$. This leads to $S_{13} = S_{23} \equiv S$, and the expressions for the vector potential simplify to

$$\mathbf{A} = \hbar\begin{pmatrix} \nabla S & -i\cos\theta\nabla\phi \\ i\cos\theta\nabla\phi & \cos^2\theta\nabla S \end{pmatrix}. \quad (89)$$

The components of the 2×2 matrix of the effective magnetic field can be easily evaluated to be

$$\mathbf{B}_{11} = 0,$$
$$\mathbf{B}_{12} = i\hbar\sin\theta e^{-iS}\nabla\theta\times\nabla\phi - \hbar\cos\theta e^{-iS}\nabla S\times\nabla\phi\left(1+\cos^2\theta\right),$$
$$\mathbf{B}_{22} = -2\hbar\cos\theta\sin\theta\nabla\theta\times\nabla S. \quad (90)$$

One recognizes that a large magnetic field requires large gradients of the relative intensities of the fields, parametrized by the angles ϕ and θ and a large gradient of the relative phase S. Gradients of ϕ and θ on the order of the wavenumber k can be achieved by using standing-wave fields. Large gradients of S can be obtained from a running wave Ω_3 orthogonal to the other two or by a vortex beam with large orbital angular momentum. In this case, magnetic fluxes as large as 1 Dirac flux quantum per atom can be reached.

We now construct a specific field configuration that leads to a magnetic monopole. For this we will consider two copropagating and circularly polarized fields $\Omega_{1,2}$ with opposite orbital angular momenta $\pm\hbar$ along the propagation axis z, whereas the third field Ω_3 propagates in x direction and is linearly polarized along the y-axis [52]:

$$\Omega_{1,2} = \Omega_0 \frac{\rho}{R} \mathrm{e}^{i(kz \mp \varphi)}, \qquad \Omega_3 = \Omega_0 \frac{z}{R} \mathrm{e}^{ik'x}. \tag{91}$$

Here ρ is the cylindrical radius, and φ is the azimuthal angle. It should be noted that these fields have a vanishing divergence and obey the Helmholtz equation. The total intensity of the laser fields (91) vanishes at the origin which is a singular point.

The vector potential associated with the fields can be calculated using equation (86):

$$\mathbf{A} = -\hbar \frac{\cos\vartheta}{r\sin\vartheta} \hat{\mathrm{e}}_\varphi \begin{pmatrix} 0 & 1 \\ 1 & 0 \end{pmatrix} + \frac{\hbar}{2}\left(k\hat{\mathrm{e}}_z - k'\hat{\mathrm{e}}_x\right) \left[\left(1+\cos^2\vartheta\right)\begin{pmatrix} 1 & 0 \\ 0 & 1 \end{pmatrix} + \left(1-\cos^2\vartheta\right)\begin{pmatrix} 1 & 0 \\ 0 & -1 \end{pmatrix}\right]. \tag{92}$$

The first term proportional to σ_x corresponds to a magnetic monopole of the unit strength at the origin. This is easily seen by calculating the magnetic field

$$\mathbf{B} = \frac{\hbar}{r^2} \hat{\mathrm{e}}_r \begin{pmatrix} 0 & 1 \\ 1 & 0 \end{pmatrix} + \cdots. \tag{93}$$

The dots indicate nonmonopole field contributions proportional to the Pauli matrices σ_z and σ_y, and to the unity matrix.

12.7 ULTRA-RELATIVISTIC BEHAVIOR OF COLD ATOMS IN LIGHT-INDUCED GAUGE POTENTIALS

12.7.1 Introduction

In this section, we will show how cold atoms can acquire properties of ultra-relativistic fermions [54] if they are manipulated properly by light fields acting upon

the atoms in the tripod configuration (see also references [51,59] for similar effects with atoms in optical lattices). Specifically, we demonstrate that by choosing certain light fields the vector potential can be made proportional to an operator of spin 1/2. For small momenta, the atomic motion becomes then equivalent to the ultra-relativistic motion of two-component Dirac fermions, as is the case also for electrons in graphene near the Fermi surface [60–68]. In this section, we will discuss an experimental setup for observing such a quasi-relativistic behavior for the cold atoms. Furthermore, we will show that the atoms can experience negative refraction and focusing by Veselago-type lenses [69,70].

It is important to realize that the velocity of the quasi-relativistic atoms is of the order of a centimeter per second. This is ten orders of magnitude smaller than the speed of light in a vacuum $c \approx 3 \times 10^8$ m/s. For comparison, the velocity of the Dirac-type electrons in graphene is only two orders of magnitude smaller than c [63]. Thus, the ultra-relativistic behavior of cold atoms manifests itself at extremely small velocities.

12.7.2 Formulation

To demonstrate the ultra-relativistic behavior of cold atoms [54], we will consider the tripod scheme where the first two lasers have the same intensities and counterpropagate in the x-direction, while the third one propagates in the negative y-direction, as shown in Figure 12.11. Specifically, we have $\Omega_1 = \Omega \sin\theta e^{-i\kappa x}/\sqrt{2}$, $\Omega_2 = \Omega \sin\theta e^{i\kappa x}/\sqrt{2}$, and $\Omega_3 = \Omega \cos\theta e^{-i\kappa y}$, where $\Omega = \sqrt{|\Omega_1|^2 + |\Omega_2|^2 + |\Omega_3|^2}$ is the total Rabi frequency and θ is the mixing angle defining the relative intensity of the third laser field.

The potentials $\mathbf{A}$, Φ, and V have been considered in the previous section for arbitrary light fields acting upon tripod atoms. In the present configuration of the light fields, the potentials take the form [54]

$$\mathbf{A} = \hbar\kappa \begin{pmatrix} \mathbf{e}_y & -\mathbf{e}_x \cos\theta \\ -\mathbf{e}_x \cos\theta & \mathbf{e}_y \cos^2\theta \end{pmatrix}, \tag{94}$$

$$\Phi = \begin{pmatrix} \hbar^2\kappa^2 \sin^2\theta/2m & 0 \\ 0 & \hbar^2\kappa^2 \sin^2(2\theta)/8m \end{pmatrix}, \tag{95}$$

$$V = \begin{pmatrix} V_1 & 0 \\ 0 & V_1 \cos^2\theta + V_3 \sin^2\theta \end{pmatrix}, \tag{96}$$

with $\mathbf{e}_x$ and $\mathbf{e}_y$ being unit Cartesian vectors. Here the external trapping potential is assumed to be the same for the first two atomic states, $V_1 = V_2$.

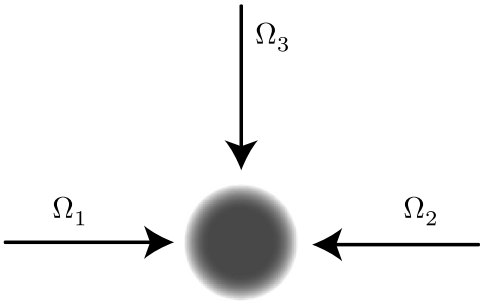

Figure 12.11 The three laser beams incident on the cloud of atoms in the tripod configuration.

In what follows, we take $V_3 - V_1 = \hbar^2\kappa^2 \sin^2(\theta)/2m$. This can be achieved by detuning the third laser from the two-photon resonance by the frequency $\Delta\omega_3 = \hbar\kappa^2 \sin^2\theta/2m$. Thus, the overall trapping potential simplifies to $V + \Phi = V_1\mathrm{I}$ (up to a constant), where I is the unit matrix. In other words, both dark states are affected by the same trapping potential $V_1 \equiv V_1(\mathbf{r})$.

Furthermore, we take the mixing angle $\theta = \theta_0$ to be such that $\sin^2\theta_0 = 2\cos\theta_0$, giving $\cos\theta_0 = \sqrt{2} - 1$. In that case, the vector potential can be represented in a symmetric way in terms of the Pauli matrices σ_x and σ_z,

$$\mathbf{A} = \hbar\kappa'(-\mathbf{e}_x\sigma_x + \mathbf{e}_y\sigma_z) + \hbar\kappa_0\mathbf{e}_y\mathrm{I}, \tag{97}$$

where $\kappa' = \kappa\cos\theta_0 \approx 0.414\kappa$ and $\kappa_0 = \kappa(1 - \cos\theta_0)$. Although the vector potential is constant, it cannot be eliminated via a gauge transformation, because the Cartesian components A_x and A_y do not commute. Thus, the light-induced potential $\mathbf{A}$ is non-Abelian. Such a non-Abelian gauge potential can also be induced in optical lattices using other techniques [50].

12.7.3 Quasi-Relativistic Behavior of Cold Atoms

It is convenient to introduce the new dark states:

$$|D_1'\rangle = \frac{1}{\sqrt{2}}\big(|D_1\rangle + i|D_2\rangle\big)e^{i\kappa_0 y}, \tag{98}$$

$$|D_2'\rangle = \frac{i}{\sqrt{2}}\big(|D_1\rangle - i|D_2\rangle\big)e^{i\kappa_0 y}. \tag{99}$$

The transformed two component wave-function is related to the original one according to $\Psi' = \exp(-i\kappa_0 y)\exp(-i\frac{\pi}{4}\sigma_x)\Psi$, where σ_x is the Pauli spin matrix. The exponential factor $\exp(-i\kappa_0 y)$ induces a shift in the origin of the momentum $\mathbf{k} \to \mathbf{k} - \kappa_0\mathbf{e}_y$.

With the new set of dark states, we get the vector potential $\mathbf{A}' = -\hbar\kappa'\sigma_\perp$, where $\sigma_\perp = \mathbf{e}_x\sigma_x + \mathbf{e}_y\sigma_y$ is the spin $\frac{1}{2}$ operator in the xy-plane. The transformed equation of the atomic motion takes the form

$$i\hbar\frac{\partial}{\partial t}\Psi' = \left[\frac{1}{2m}(-i\hbar\nabla + \hbar\kappa'\boldsymbol{\sigma}_\perp)^2 + V_1\right]\Psi'. \tag{100}$$

In this way, the vector potential governing the atomic motion is proportional to the spin operator $\sigma_\perp$.

If the trapping potential V_1 is constant, we can consider plane-wave solutions,

$$\Psi'(\mathbf{r}, t) = \Psi_\mathbf{k} e^{i\mathbf{k}\cdot\mathbf{r} - i\omega_\mathbf{k} t}, \quad \Psi_\mathbf{k} = \begin{pmatrix} \Psi_{1\mathbf{k}} \\ \Psi_{2\mathbf{k}} \end{pmatrix}, \tag{101}$$

where $\omega_\mathbf{k}$ is the eigen-frequency. The $\mathbf{k}$-dependent spinor $\Psi_\mathbf{k}$ obeys the stationary Schrödinger equation $H_\mathbf{k}\Psi_\mathbf{k} = \hbar\omega_\mathbf{k}\Psi_\mathbf{k}$, with the following $\mathbf{k}$-dependent Hamiltonian

$$H_\mathbf{k} = \frac{\hbar^2}{2m}(\mathbf{k} + \kappa'\boldsymbol{\sigma}_\perp)^2 + V_1. \tag{102}$$

For small wave-vectors ($k \ll \kappa'$), the atomic Hamiltonian reduces to the Hamiltonian for the 2D relativistic motion of a two-component massless particle of the Dirac type,

$$H_\mathbf{k} = \hbar v_0 \mathbf{k}\cdot\boldsymbol{\sigma}_\perp + V_1 + m v_0^2, \tag{103}$$

where $v_0 = \hbar\kappa'/m$ is the velocity of such a quasi-relativistic particle. The velocity v_0 represents the recoil velocity corresponding to the wave-vector κ' and is typically of the order of a centimeter per second.

The Hamiltonian $H_\mathbf{k}$ commutes with the 2D chirality operator $\sigma_\mathbf{k} = \mathbf{k}\cdot\boldsymbol{\sigma}_\perp/k$. The latter is characterized by the eigenstates

$$\Psi_\mathbf{k}^\pm = \frac{1}{\sqrt{2}}\begin{pmatrix} 1 \\ \pm\frac{k_x + ik_y}{k} \end{pmatrix}, \tag{104}$$

for which $\sigma_\mathbf{k}\Psi_\mathbf{k}^\pm = \pm\Psi_\mathbf{k}^\pm$. The eigenstates (104) are also eigenstates of the Hamiltonian $H_\mathbf{k}$ with eigen-frequencies $\omega_\mathbf{k} \equiv \omega_\mathbf{k}^\pm$. In the following, the atomic motion is assumed to be confined in the xy-plane. The dispersion is then given by

$$\hbar\omega_\mathbf{k}^\pm = \hbar v_0\left(k^2/2\kappa' \pm k\right) + V_1 + m v_0^2, \tag{105}$$

where the upper (lower) sign corresponds to the upper (lower) dispersion branch. The atomic motion in different dispersion branches is characterized by opposite chirality if the direction $\mathbf{k}/k$ is fixed. For small wave-vectors ($k \ll \kappa'$), the dispersion simplifies to $\hbar\omega_\mathbf{k}^\pm = \pm\hbar v_0 k + V_1 + m v_0^2$, where the upper (lower) sign corresponds to a linear cone with a positive (negative) group velocity, $v_g^\pm = \pm v_0$. Exactly the same dispersion is featured for electrons near the Fermi level in graphene [60–64].

12.7.4 Proposed Experiment

To observe the quasi-relativistic behavior of cold atoms, the following experimental situation has been proposed [54]. Suppose that initially an atom (or a dilute atomic cloud) is in the internal state $|3\rangle$ with a translational motion described by a wave-packet with a central wave-vector $\mathbf{k}_{\rm in}$ and a wave-vector spread $\Delta k \ll k_{\rm in}$. The full initial state-vector is then given by $|\Psi_{\rm in}\rangle = \psi(\mathbf{r})e^{i\mathbf{k}_{\rm in}\cdot\mathbf{r}}|3\rangle$, where the envelope function $\psi(\mathbf{r})$ varies slowly within the wavelength $\lambda_{\rm in} = 2\pi/k_{\rm in}$. The cold atoms can be set in motion using various techniques, e.g., by means of the two-photon scattering that induces a recoil momentum $\hbar\mathbf{k}_{in} = \hbar\mathbf{k}_{2\rm phot}$ to the atoms, where $\mathbf{k}_{2\rm phot}$ is a wave-vector of the two-photon mismatch.

Initially, all three lasers are off. Subsequently, the lasers are switched on in a counterintuitive manner, switching the lasers 1 and 2 on first, followed by the laser 3. At the beginning of this stage, the internal state $|3\rangle$ coincides with the dark state $|D_2\rangle$, so the full initial state-vector can be rewritten as $|\Psi_{\rm in}\rangle = \psi(\mathbf{r})e^{i\mathbf{k}_{\rm in}\cdot\mathbf{r}}|D_2\rangle$. If the laser 3 is switched on sufficiently slowly, the atom remains in the dark state $|D_2\rangle$ during the whole switch-on stage. Yet the duration of the switching on should be sufficiently short to prevent the dynamics of the atomic center of mass at this stage. Immediately after the lasers reach their steady state, the multicomponent wave-function reads:

$$\Psi = \begin{pmatrix} 0 \\ 1 \end{pmatrix} \psi(\mathbf{r})e^{i\mathbf{k}_{\rm in}\cdot\mathbf{r}}. \tag{106}$$

Expressing $|D_2\rangle$ as a function of $|D'_{1,2}\rangle$, the transformed multicomponent wave-function takes the form

$$\Psi' = \frac{1}{\sqrt{2}} \begin{pmatrix} -i \\ 1 \end{pmatrix} \psi(\mathbf{r})e^{i\mathbf{k}_c\cdot\mathbf{r}}, \tag{107}$$

where $\mathbf{k} = \mathbf{k}_{\rm in} - \kappa_0\mathbf{e}_y$ is the central wave-vector.

Let us now consider the subsequent atomic dynamics in the laser fields. As mentioned earlier in this section, to have ultra-relativistically behaving atoms, the wave-number k should be small ($k \ll \kappa$) so that $\mathbf{k}$ is a small addition to $\mathbf{k}_{\rm in} = \kappa_0\mathbf{e}_y + \mathbf{k}$. Furthermore, the wave-vector spread $\Delta k \ll k$, i.e., the width of the atomic wave-packet, is much larger than the central wavelength. Hence, the dynamics is sensitive to the direction of the central wave-vector $\mathbf{k}$. To illustrate this we will consider two specific cases.

(i) If $\mathbf{k} = \pm k\mathbf{e}_y$, the wave-function (107) can be represented as:

$$\Psi' = -i\Psi^{\pm}_{\mathbf{k}}\psi(\mathbf{r})e^{\pm iky}, \quad \Psi^{\pm}_{\mathbf{k}} = \frac{1}{\sqrt{2}} \begin{pmatrix} 1 \\ i \end{pmatrix}. \tag{108}$$

The upper (lower) sign in $\mathbf{k} = \pm k\mathbf{e}_y$ corresponds to a situation where the atom is characterized by a positive (negative) chirality, hence being in the upper (lower) dispersion branch. In both cases, the atomic wave-packet propagates along the y axis with the velocity $\mathbf{v}_0 = \mathbf{e}_y \hbar\kappa'/m$.

(ii) If the wave-vector is along the x-axis ($\mathbf{k} = k\mathbf{e}_x$), the multicomponent wavefunction (107) takes the form

$$\Psi' = \left(c_+ \Psi_{\mathbf{k}}^+ + c_- \Psi_{\mathbf{k}}^-\right)\psi(\mathbf{r})e^{i\mathbf{k}\cdot\mathbf{r}}, \quad \Psi_{\mathbf{k}}^{\pm} = \frac{1}{\sqrt{2}}\begin{pmatrix} 1 \\ \pm 1 \end{pmatrix}, \tag{109}$$

where $c_\pm = (-i \pm 1)/2$. In this case, the initial wave-packet splits into two with equal weights ($|c_\pm^2| = 1/2$) and the same wave-vector $\mathbf{k}$. The two wave-packets are characterized by the different chiralities and thus move in opposite directions. The wave-packet with a positive chirality (plus sign in $\Psi_{\mathbf{k}}^{\pm}$) belongs to the upper dispersion branch and moves along the x-axis with a velocity $\mathbf{v}_0 = \mathbf{e}_x \hbar\kappa'/m$. On the other hand, the wave-packet characterized by a negative chirality (minus sign in $\Psi_{\mathbf{k}}^{\pm}$) moves with a velocity $\mathbf{v}_0 = -\mathbf{e}_x \hbar\kappa'/m$.

Suppose the time is sufficiently small ($v_0 t < d$) so the wave-packets of the width d are not yet spatially separated. The internal atomic state will then undergo temporal oscillations between the dark states $|D_2\rangle$ and $|D_1\rangle$, with a frequency equal to $\omega_{\mathbf{k}}^+ - \omega_{\mathbf{k}}^- = 2v_0 k$. Such an internal dynamics can be detected by switching the laser 3 off at a certain time. This transforms the dark state $|D_2\rangle$ to the physical state $|3\rangle$. Subsequently, one can measure the population of the state $|3\rangle$ for various delay times and various wave-vectors $\mathbf{k}$. The chiral nature of the atomic motion will manifest itself in the oscillations of the population of the atomic state $|3\rangle$ if $\mathbf{k}$ is along the x-axis, and the absence of such oscillations if $\mathbf{k}$ is along the y-axis.

Furthermore, as a consequence of the constructed Hamiltonian (103), the quasi-relativistic atoms can show negative refraction at a potential barrier and thus exhibit focusing by Veselago-type lenses [69,70]. Consider incident atoms that are in the upper dispersion branch and propagate along the y-axis with a wave-vector $\mathbf{k} = k\mathbf{e}_y$. Let us place a potential barrier of a height $2\hbar v_0 k$ at an angle of incidence α, as shown in Figure 12.12. Inside the barrier, the atoms are transferred to the lower dispersion branch with $\mathbf{k}_t = -k[\cos(2\alpha)\mathbf{e}_y + \sin(2\alpha)\mathbf{e}_x]$. This would lead to the negative refraction of cold atoms at the barrier as shown in Figure 12.12. Thus, the potential barrier can act as a flat lens that refocuses the atomic wave-packet.

In this way, we have shown how the atomic motion can be equivalent to the dynamics of ultra-relativistic (massless) two-component Dirac fermions. As a result, the ultracold atoms can experience negative refraction and focusing by Veselago-type lenses. In addition, the chiral nature of the atomic motion is manifested through dy-

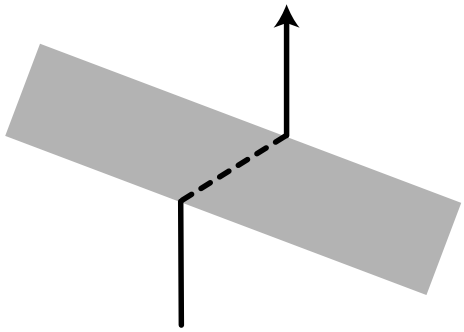

Figure 12.12 Negative refraction of cold atoms at a potential barrier. The incoming and outgoing atoms are in the upper dispersion branch with a wave-vector $\mathbf{k}$ (solid line), whereas the atoms inside the barrier are in a lower dispersion branch with a wave-vector $\mathbf{k}_t$ (dashed line).

namics of the population of the internal atomic states, which is highly sensitive to the direction of the center of mass motion.

12.8 FINAL REMARKS

In this chapter, we have considered different types of manipulation of cold atoms by light fields. We have reviewed the mechanisms for trapping ensembles of ultracold atoms. The optical trap formed the basis for manipulating the cold atoms where we relied upon on the coherent nature of the ultracold sample of atoms and the intensity of the light.

Subsequently, we have discussed a situation where the phase and the intensity of the incident light both play a crucial role, i.e., we have considered a different kind of optical manipulation where the laser fields are applied to induce vector and scalar potentials for the atoms. The induced potentials have a geometric nature and depend exclusively upon the relative intensity and relative phase of the laser beams involved rather on their absolute intensity. The approach relies on the ability to prepare the atoms in superpositions of the internal energy states of the atom.

The technique provides a way to optically produce an effective magnetic field acting upon electrically neutral atoms. This happens if the applied laser fields have a nontrivial topology (e.g., if they carry an orbital angular momentum along the propagation direction [5–7,34,35]) or if the atom-light system contains more than one degenerate dark state. The latter situation appears in the tripod configuration of the light-atom system exhibiting two degenerate dark states. Consequently, the light-induced potentials are 2×2 matrices, whose Cartesian components generally do not commute [52,

54], i.e., the potentials are non-Abelian. In such a situation, nontrivial light-induced gauge potentials can be produced, even using plane waves.

Finally, we noted that the tripod scheme of the light-matter coupling can have other important applications, e.g., it can be used to produce solitons in atomic Bose–Einstein condensates [71]. Using this method, it is possible to circumvent the restriction set by the diffraction limit inherent to conventional methods, such as the phase imprinting [24,25].

REFERENCES

[1] J.D. Jackson, Classical Electrodynamics, Wiley, New York, 1998.
[2] P. Meystre, Atom Optics, American Institute of Physics, 2001.
[3] C.J. Pethick, H. Smith, Bose–Einstein Condensation in Dilute Gases, Cambridge Univ. Press, Cambridge, 2001.
[4] L.P. Pitaevskii, S. Stringari, Bose–Einstein Condensation, Clarendon Press, Oxford, 2003.
[5] G. Juzeliūnas, P. Öhberg, Slow light in degenerate Fermi gases, *Phys. Rev. Lett. 93* (2004) 033602.
[6] G. Juzeliūnas, P. Öhberg, J. Ruseckas, A. Klein, Effective magnetic fields in degenerate atomic gases induced by light beams with orbital angular momenta, *Phys. Rev. A 71* (2005) 053614.
[7] G. Juzeliūnas, J. Ruseckas, P. Öhberg, Effective magnetic fields induced by eit in ultra-cold atomic gases, *J. Phys. B 38* (2005) 4171.
[8] S. Stenholm, The semiclassical theory of laser cooling, *Rev. Mod. Phys. 58* (1986) 699.
[9] R.J. Cook, Atomic motion in resonant radiation: An application of Ehrenfest's theorem, *Phys. Rev. A 20* (1979) 224.
[10] C. Cohen-Tannoudji, J. Dupont-Roc, G. Grynberg, Atom–Photon Interactions, Wiley, New York, 1998.
[11] S.M. Barnett, P.M. Radmore, Methods in Theoretical Quantum Optics, Clarendon Press, Oxford, 1997.
[12] R. Loudon, The Quantum Theory of Light, Oxford Univ. Press, 1979.
[13] M.H. Anderson, J.R. Ensher, M.R. Matthews, C.E. Wieman, E.A. Cornell, Observation of Bose–Einstein condensation in a dilute atomic vapor, *Science 269* (1995) 198.
[14] K.B. Davis, M.-O. Mewes, M.R. Andrews, N.J. van Druten, D.S. Durfee, D.M. Kurn, W. Ketterle, Bose–Einstein condensation in a gas of sodium atoms, *Phys. Rev. Lett. 75* (1995) 3969.
[15] C.C. Bradley, C.A. Sackett, J.J. Tollett, R.G. Hulet, Evidence of Bose–Einstein condensation in an atomic gas with attractive interactions, *Phys. Rev. Lett. 75* (1995) 1687.
[16] J. Stenger, S. Inouye, M. Andrews, H.-J. Miesner, D. Stamper-Kurn, W. Ketterle, Strongly enhanced inelastic collisions in a Bose–Einstein condensate near Feshbach resonances, *Phys. Rev. Lett. 82* (1999) 2422.
[17] S.N. Bose, Plancks Gesetz und Lichtquantenhypothese, *Z. Phys. 26* (1924) 178.
[18] A. Einstein, Quantentheorie des einatomigen Idealen Gases, *Sitzungsber. Kgl. Preuss. Akad. Wiss. 3* (1924) 261.
[19] F. London, The λ-phenomenon of liquid helium and the Bose–Einstein degeneracy, *Nature 141* (1938) 643.
[20] K. Huang, Statistical Mechanics, Wiley, New York, 1987.

[21] D. Kleppner, in: M. Inguscio, S. Stringari, C. Wieman (Eds.), *Bose–Einstein Condensation in Atomic Gases: Enrico Fermi International School of Physics*, IOS Press, US, 1999.

[22] A.S. Arnold, C.S. Garvie, E. Riis, Large magnetic storage ring for Bose–Einstein condensates, *Phys. Rev. A 73* (2006) 041606.

[23] G. Baym, C.J. Pethick, Ground-state properties of magnetically trapped Bose-condensed rubidium gas, *Phys. Rev. Lett. 76* (1996) 6.

[24] S. Burger, K. Bongs, S. Dettmer, W. Ertmer, K. Sengstock, A. Sanpera, G.V. Shlyapnikov, M. Lewenstein, Dark solitons in Bose–Einstein condensates, *Phys. Rev. Lett. 83* (1999) 5198.

[25] J. Denschlag, J.E. Simsarian, D.L. Feder, C.W. Clark, L.A. Collins, J. Cubizolles, L. Deng, E.W. Hagley, K. Helmerson, W.P. Reinhardt, S.L. Rolston, B.I. Schneider, W.D. Phillips, Generating solitons by phase engineering of a Bose–Einstein condensate, *Science 287* (2000) 97.

[26] M.D. Girardeau, E.M. Wright, Breakdown of time-dependent mean-field theory for a one-dimensional condensate of impenetrable bosons, *Phys. Rev. Lett. 84* (2000) 5239.

[27] G. Whyte, P. Öhberg, J. Courtial, Transverse laser modes in Bose–Einstein condensates, *Phys. Rev. A 69* (2004) 053610.

[28] D.R. Murray, P. Öhberg, Matter wave focusing, *J. Phys. B 38* (2005) 1227.

[29] E. Arimondo, Coherent population trapping in laser spectroscopy, *Prog. Opt. 35* (1996) 259.

[30] S.E. Harris, Electromagnetically induced transparency, *Phys. Today 50* (1997) 36.

[31] A.B. Matsko, O. Kocharovskaja, Y. Rostovtsev, G.R. Welch, A.S. Zibrov, M.O. Scully, Slow, ultraslow, stored, and frozen light, *Adv. At. Mol. Opt. Phys. 46* (2001) 191.

[32] M.D. Lukin, Trapping and manipulating photon states in atomic ensembles, *Rev. Mod. Phys. 75* (2003) 457.

[33] M. Fleischhauer, A. Imamoglu, J.P. Maragos, Electromagnetically induced transparency: Optics in coherent media, *Rev. Mod. Phys. 77* (2005) 633.

[34] G. Juzeliūnas, P. Öhberg, Creation of effective magnetic fields using electromagnetically induced transparency, *Opt. Spectroscopy 99* (2005) 357.

[35] P. Öhberg, G. Juzeliūnas, J. Ruseckas, M. Fleischhauer, Filled landau levels in neutral quantum gases, *Phys. Rev. A 72* (2005) 053632.

[36] M.V. Berry, Quantal phase factors accompanying adiabatic changes, *Proc. R. Soc. A 392* (1984) 45.

[37] C.A. Mead, The geometric phase in molecular systems, *Rev. Mod. Phys. 64* (1992) 51.

[38] F. Wilczek, A. Zee, Appearance of gauge structure in simple dynamical systems, *Phys. Rev. Lett. 52* (1984) 2111.

[39] J. Moody, A. Shapere, F. Wilczek, Realizations of magnetic-monopole gauge fields: Diatoms and spin precession, *Phys. Rev. Lett. 56* (1986) 893.

[40] R. Jackiw, Berry's phase-topological ideas from atomic, molecular and optical physics, *Comments At. Mol. Phys. 21* (1988) 71.

[41] C.-P. Sun, M.-L. Ge, Generalizing Born–Oppenheimer approximations and observable effects of an induced gauge field, *Phys. Rev. D 41* (1990) 1349.

[42] R. Dum, M. Olshanii, Gauge structures in atom–laser interaction: Bloch oscillations in a dark lattice, *Phys. Rev. Lett. 76* (1996) 1788.

[43] P.M. Visser, G. Nienhuis, Geometric potentials for subrecoil dynamics, *Phys. Rev. A 57* (1998) 4581.

[44] V. Bretin, S. Stock, Y. Seurin, J. Dalibard, Fast rotation of a Bose–Einstein condensate, *Phys. Rev. Lett. 92* (2004) 050403.

[45] V. Schweikhard, I. Coddington, P. Engels, V.P. Mogendorff, E.A. Cornell, Rapidly rotating Bose–Einstein condensates in and near the lowest landau level, *Phys. Rev. Lett. 92* (2004) 040404.
[46] M.A. Baranov, K. Osterloh, M. Lewenstein, Fractional quantum hall states in ultracold rapidly rotating dipolar Fermi gases, *Phys. Rev. Lett. 94* (2004) 070404.
[47] D. Jaksch, P. Zoller, Creation of effective magnetic fields in optical lattices: The Hofstadter butterfly for cold neutral atoms, *New J. Phys. 5* (2003) 56.
[48] E.J. Mueller, Artificial electromagnetism for neutral atoms: Escher staircase and laughlin liquids, *Phys. Rev. A 70* (2004) 041603.
[49] A.S. Sørensen, E. Demler, M.D. Lukin, Fractional quantum hall states of atoms in optical lattices, *Phys. Rev. Lett. 94* (2005) 086803.
[50] K. Osterloh, M. Baig, L. Santos, P. Zoller, M. Lewenstein, Cold atoms in non-Abelian gauge potentials: From the Hofstadter moth to lattice gauge theory, *Phys. Rev. Lett. 95* (2005) 010403.
[51] J. Ruostekoski, G.V. Dunne, J. Javanainen, Particle number fractionalization of an atomic Fermi–Dirac gas in an optical lattice, *Phys. Rev. Lett. 88* (2002) 180401.
[52] J. Ruseckas, G. Juzeliūnas, P. Öhberg, M. Fleischhauer, Non-Abelian gauge potentials for ultracold atoms with degenerate dark states, *Phys. Rev. Lett. 95* (2005) 010404.
[53] G. Juzeliūnas, J. Ruseckas, P. Öhberg, M. Fleischhauer, Light-induced effective magnetic fields for ultracold atoms in planar geometries, *Phys. Rev. A 73* (2006) 025602.
[54] G. Juzeliunas, J. Ruseckas, M. Lindberg, L. Santos, P. Öhberg, Quasi-relativistic behavior of cold atoms in light fields, *Phys. Rev. A 77* (2008) 011802(R).
[55] L.V. Hau, Z. Dutton, C. Behrooz, Light speed reduction to 17 metres per second in an ultracold atomic gas, *Nature 397* (1999) 594.
[56] L. Allen, M. Padgett, M. Babiker, The orbital angular momentum of light, *Prog. Opt. 39* (1999) 291.
[57] L. Allen, S.M. Narnett, M. Padgett, Optical Angular Momentum, Institute of Physics, Bristol, 2003.
[58] R.G. Unanyan, M. Fleischhauer, B.W. Shore, K. Bergmann, Robust creation and phase-sensitive probing of superposition states via stimulated Raman adiabatic passage (stirap) with degenerate dark states, *Opt. Commun. 155* (1998) 144.
[59] S.L. Zhu, B. Wang, L.-M. Duan, Simulation and detection of Dirac fermions with cold atoms in an optical lattice, *Phys. Rev. Lett. 98* (2007) 260402.
[60] K.S. Novoselov, A.K. Geim, S.V. Morozov, D. Jiang, M.I. Katsnelson, I.V. Grigorieva, S.V. Dubonos, A.A. Firsov, Two-dimensional gas of massless Dirac fermions in graphene, *Nature 438* (2005) 197.
[61] E. McCann, V.I. Fal'ko, Landau-level degeneracy and quantum hall effect in a graphite bilayer, *Phys. Rev. Lett. 96* (2006) 086805.
[62] M.I. Katsnelson, K.S. Novoselov, A.K. Geim, Chiral tunneling and the Klein paradox in graphene, *Nature Phys. 2* (2006) 620.
[63] A.K. Geim, K.S. Novoselov, The rise of graphene, *Nature Mater. 6* (2007) 183.
[64] K.S. Novoselov, Room-temperature quantum hall effect in graphene, *Science 315* (2007) 1379.
[65] A. Matulis, F.M. Peeters, Appearance of enhanced Weiss oscillations in graphene: Theory, *Phys. Rev. B 75* (2007) 125429.
[66] R. Jackiw, S.-Y. Pi, Chiral gauge theory for graphene, *Phys. Rev. Lett. 98* (2007) 266402.
[67] J.B. Pendry, Negative refraction for electrons?, *Science 315* (2007) 1226.
[68] V.V. Cheianov, V. Fal'ko, B.L. Altshuler, The focusing of electron flow and a veselago lens in graphene $p - n$ junctions, *Science 315* (2007) 1252.

[69] V.G. Veselago, The electrodynamics of substances with simultaneously negative values of ε and μ, *Sov. Phys. Usp. 10* (1968) 509.

[70] J.B. Pendry, Negative refraction makes a perfect lens, *Phys. Rev. Lett. 85* (2000) 3966.

[71] G. Juzeliūnas, J. Ruseckas, P. Öhberg, M. Fleischhauer, Formation of solitons in atomic Bose–Einstein condensates by dark-state adiabatic passage, *Lithuanian J. Phys. 47* (2007) 357.